3.5. Supplemental surface geoscientific survey in Kinigi

3.5.1. Geological Survey in Kinigi

(1) Results of remote sensing analysis and geological survey

1) Kinigi field

Kinigi field is located in the eastern part of Virunga Volcanic Range (hereinafter, VVR) where volcanos of the late Quaternary are distributed. The location map of this field is shown in Fig. 3-5.1. From the west to the north, this field is surrounded by the volcanos of the VVR, Mt. Karisimbi (Elevation: 4,507m) in the west, Mt. Visoke (3,711m) in the northwest, Mt. Sabyinyo (3,645m) in the north, and Mt. Gahinga (3,474m) in the northeast. Excluding Mt. Sabyinyo, which has an eroded mountain shape, the other volcanos have a conical and smooth mountain shape with an extended skirt. Between Mt. Visoke and Mt. Sabyinyo, many volcanic cones are aligned in a NE-SW direction. The central part of this field corresponds to the skirts of the volcanos mentioned above, and consists of flat terrain which is covered by lava flows that have erupted at intervals and debris flow sediments. In the southern part of this field, which has a steep and rough terrain, the basement complex consists of Proterozoic metamorphic and plutonic rocks which are exposed. Also, the terrain of the southern part reflects the geological structures of the basement complex, and its mountain ridges and valleys are extended in a N-S and NNW-SSW direction.

2) Remote sensing study

A remote sensing study using satellite imagery data acquired by earth observation satellites and a digital elevation model (hereinafter, DEM) was carried out to extract information related to geothermal manifestations (fractures, altered minerals, thermal anomalies, and so on) in the Kinigi field. Thick coverage of vegetation and clouds made it difficult to obtain information related to altered minerals and thermal anomalies by using optical sensor image data (Landsat-7/ETM+, Landsat-8/OLI, and Terra/ASTER) in the 2nd Phase of this study. Therefore, the processed images from synthetic aperture radar (hereinafter, SAR) and DEM were applied mainly to lineament interpretation to extract information regarding fractures in this field. The ALOS/PALSAR image, ASTER/GDEM color shade image and ASTER/GDEM overlaid image of slope analysis and shaded relief image are shown in Fig. 3-5.2 to Fig. 3-5.4, and the result of lineament interpretation using these processed images is shown in Fig. 3-5.5.

It was difficult to detect a lineament based on geographical characteristics due to the fact that the central part of this field consists of flat terrain, as mentioned in the previous paragraph. On the other hand, the extraction of lineaments is possible for the volcanic terrains of the northern part of the field based on its geographical features (alignment of volcanic cones, etc.), and NW-SE and NE-SW lineaments dominate. In the southern part of this field, NNW-SSE lineaments dominate, and threnddirection trend harmonizes with the orientation of the geological structure.

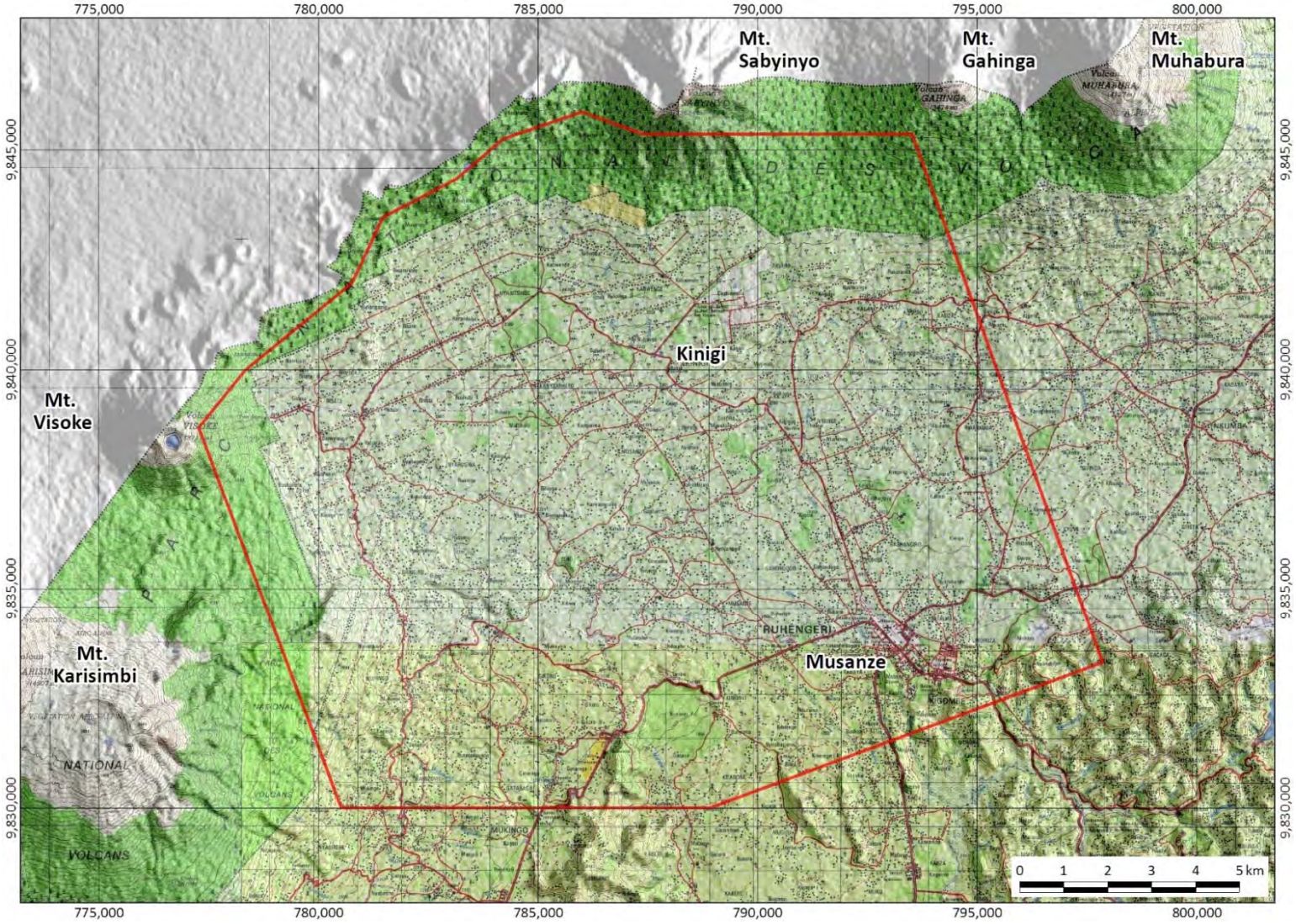

Source: JICA study team

Fig. 3-5.1 Location map of Kinigi field

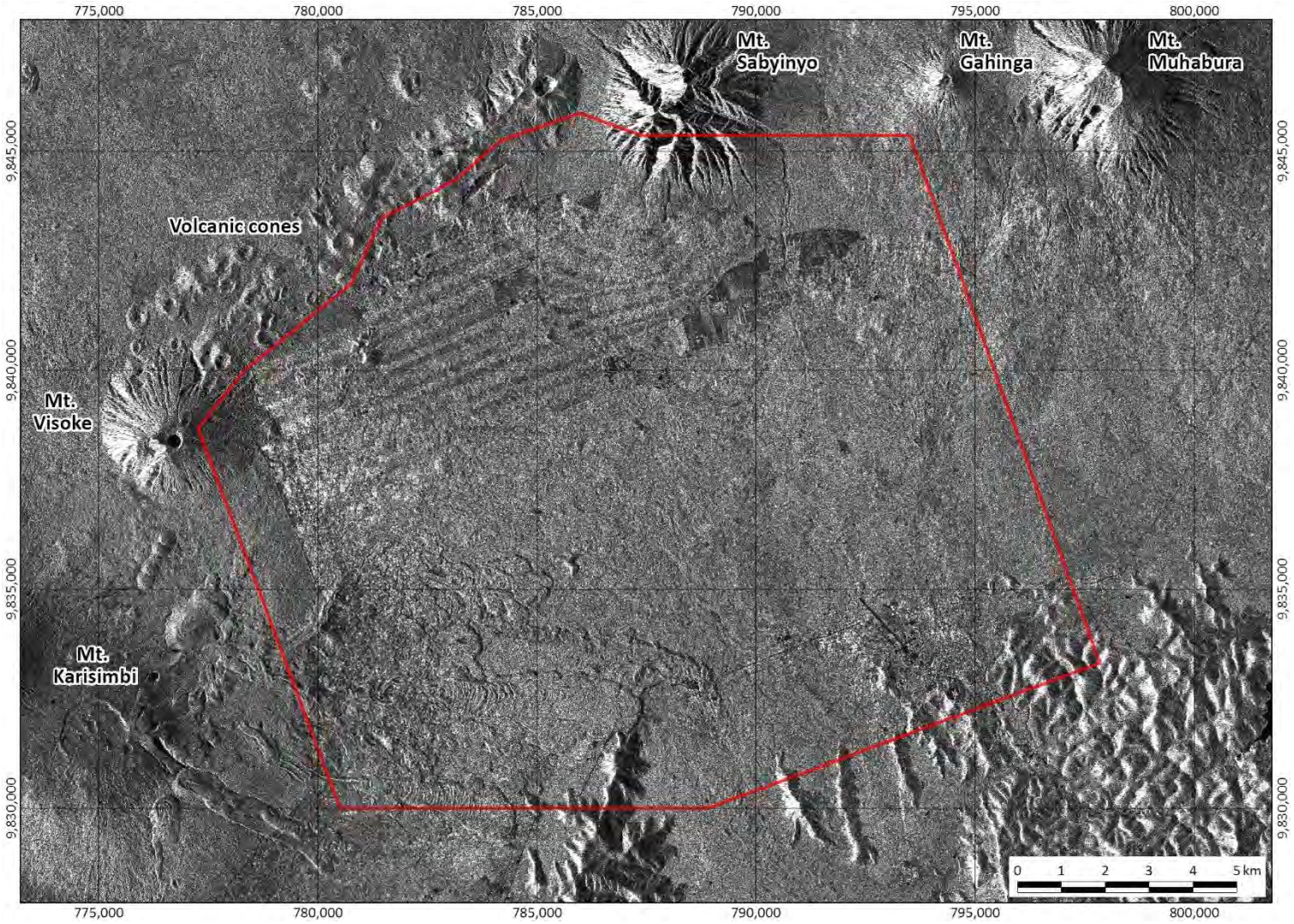

Source: JICA study team

Fig. 3-5.2 ALOS/PALSAR image of Kinigi field

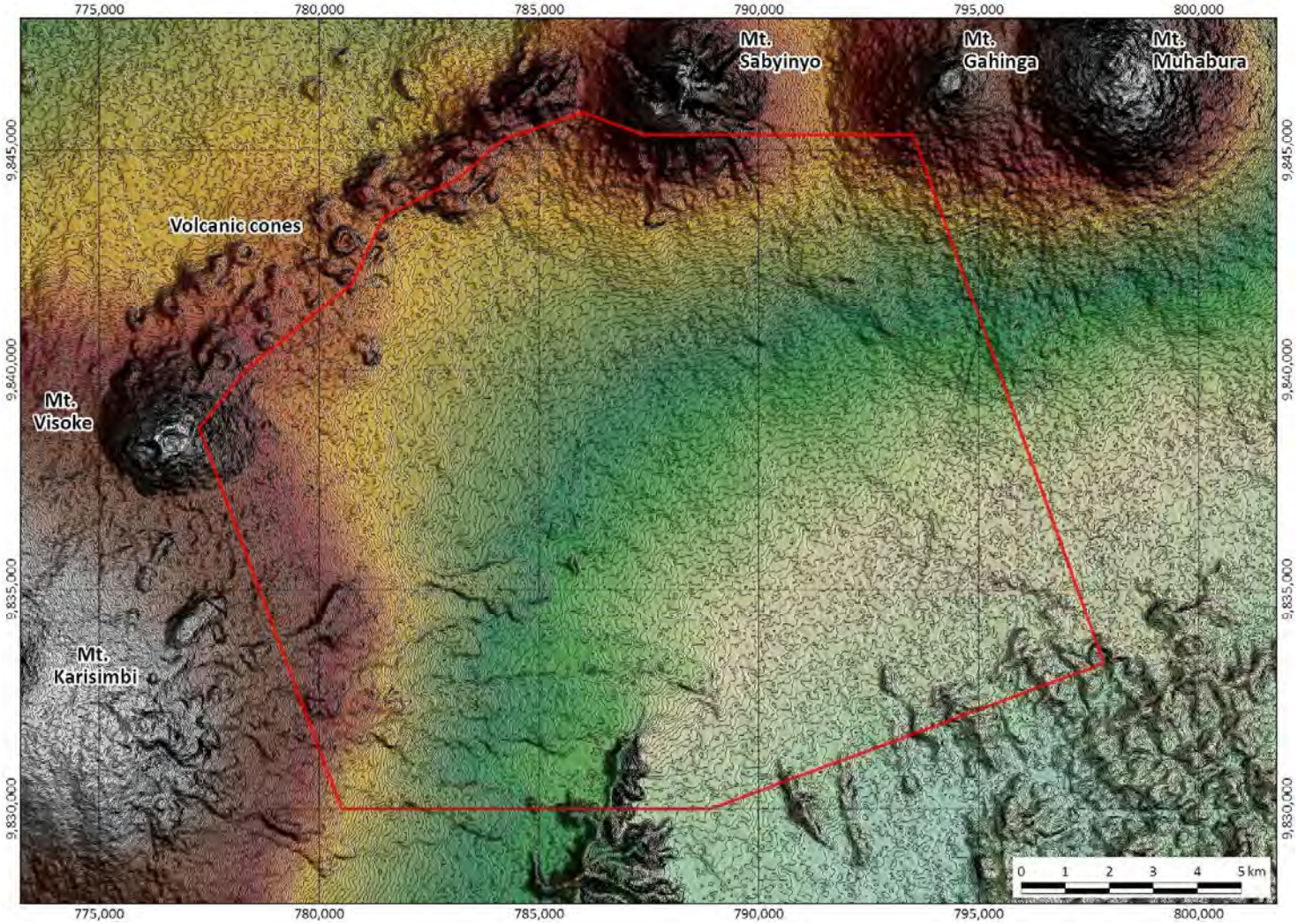

Source: JICA study team

Fig. 3-5.3 ASTER/GDEM color shaded image of Kinigi field

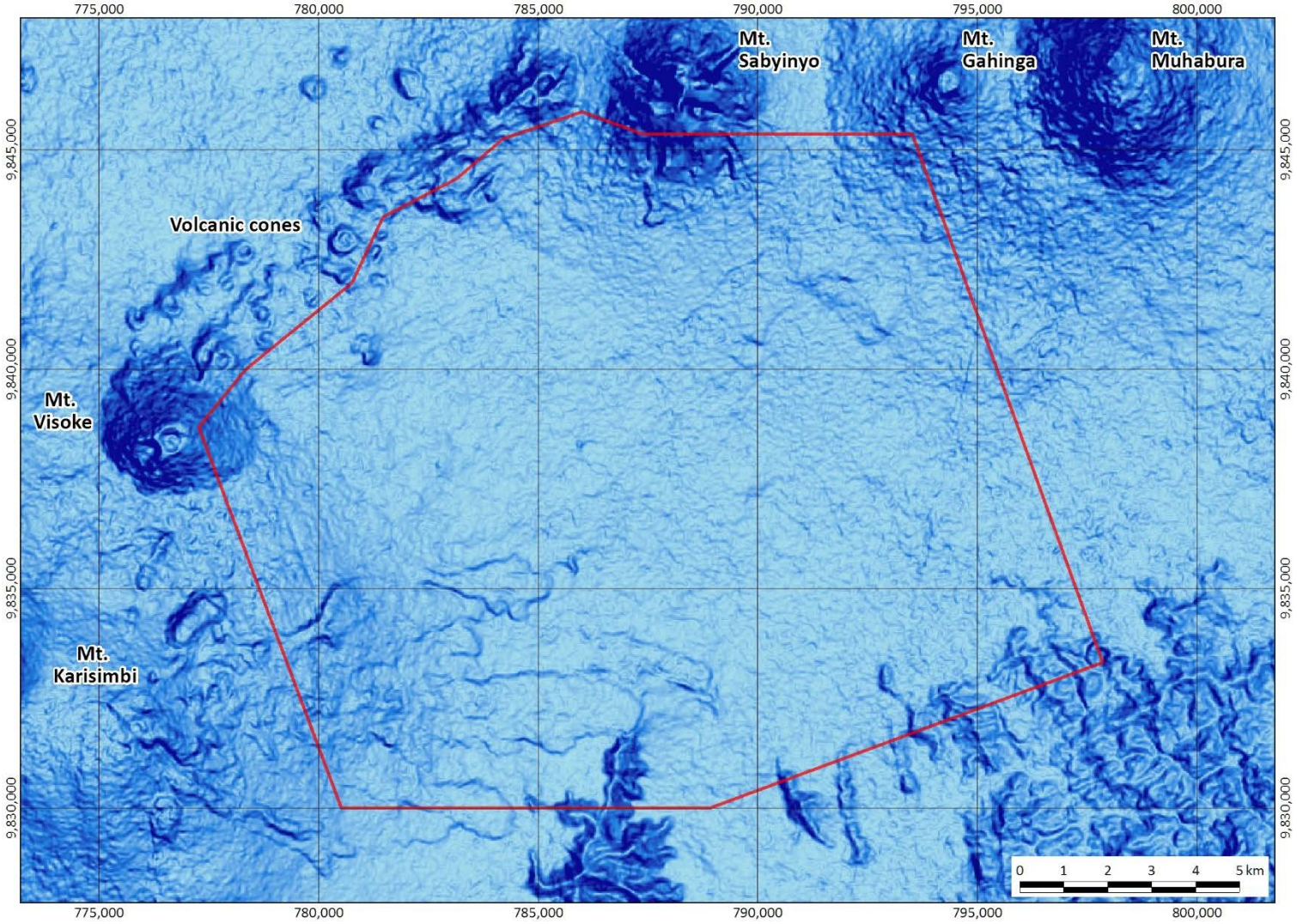

Source: JICA study team

Fig. 3-5.4 ASTER/GDEM overlaid image of slope analysis and shaded relief image of Kinigi field

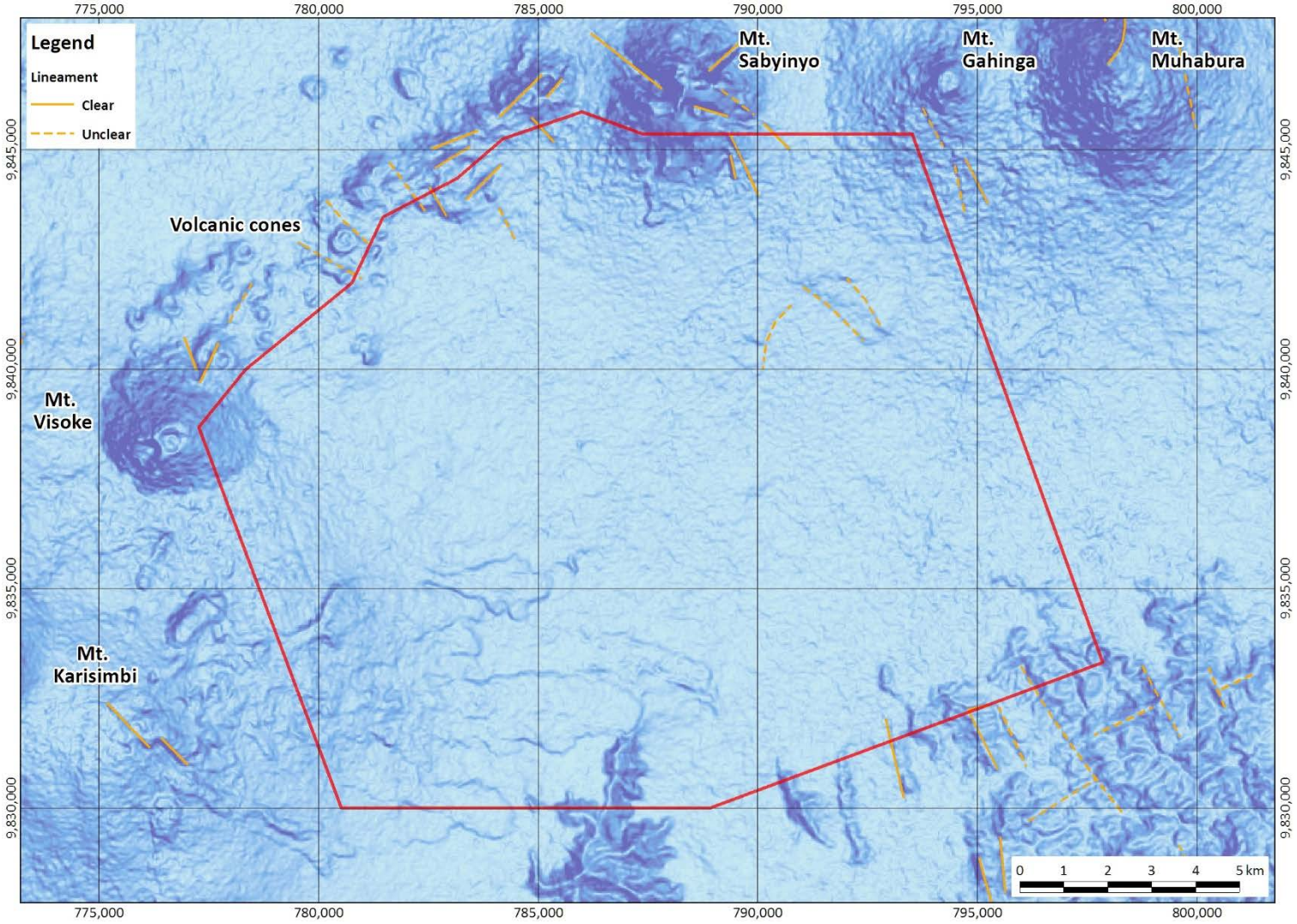

Source: JICA study team

Fig. 3-5.5 Result of lineament interpretation for Kinigi field

3) Geological survey

A geological survey was carried out to obtain supplemental data for updating of the geothermal conceptual model of Kinigi field, to validate the results of the remote sensing study, and to collect samples for laboratory analysis. The members of study team formed for the geological survey are as follows:

JICA study team : T. YAHARA, T. KOSEKI and S. KAGEYAMA
REG / GU : Jean Pascal NIYIGENA and Eugene KARANGWA

The location map of survey points is shown in Fig. 3-5.6. This survey was performed for 7 days, from 27th August to 2nd September 2015 at 35 survey points. At 31 of the survey points, macroscopic observation for exposed rocks was carried out, and lithofacies were divided into 8 units as follows:

Volcanic rock : Karisimbi volcanic rock (Karisimbi V.), Visoke volcanic rock (Visoke V.), Sabyinyo volcanic rock 1 (Sabyinyo V. 1), Sabyinyo volcanic rock 2 (Sabyinyo V. 2), Gahinga volcanic rock (Gahinga V.), cone volcanic rock 1 (Cone V. 1), cone volcanic rock 2 (Cone V. 2)
Pyroclastic rock (Pyroclastics)
Basement rock (Basement)

At 5 of the survey points, 2 samples used for laboratory analysis (petrographic observation and K-Ar rock dating) were collected at each point. The results of the geological survey are shown in Fig. 3-5.7.

(2) **Laboratory analysis**

1) Petrographic observation

The results of polarization microscopic observation of thin sections prepared from collected samples in the geological survey are shown in Table 3-5.1, and the observations are summarized in the following paragraphs. . In addition, microphotographs of each thin section are shown in the Appendix 2-5.

0872701-T: This sample (Visoke V.), collected on the eastern slope of Mt. Visoke, is andesite. The phenocrysts consist of leucite, orthopyroxene, clinopyroxene, and opaque mineral. The granular crystals of leucite have a maximum particle diameter of 1.1mm and an average diameter of 0.5 to 1.0mm. The groundmass contains some plagioclase and orthopyroxene of < 0.2mm particle diameter and contains traces of opaque mineral. Noticeable alteration is not recognized in the phenocrysts or groundmass.

082802-T: This sample (Sabyinyo V. 2), collected on the southern slope of Mt. Sabyinyo, is andesite. The phenocrysts consist of plagioclase, biotite, orthopyroxene, clinopyroxene, and opaque mineral. The groundmass with clear fluidal texture mainly contains plagioclase of < 0.1mm particle diameter, and contains traces of pyroxene, biotite, and opaque mineral. Some of the biotite has turned brown, but noticeable alteration is not recognized.

083002-T: This sample (Sabyinyo V. 1), collected on the southeastern part of Mt. Sabyinyo, is basalt. The phenocrysts consist of plagioclase, orthopyroxene, olivine, and opaque mineral. The groundmass mainly contains plagioclase of < 0.1mm particle diameter, and contains some pyroxene and traces of olivine.

Noticeable alteration is not recognized in the phenocrysts and groundmass.

083101-T: This sample (cone V. 2), collected on the southern slope of the volcanic cones, is basalt. The phenocrysts consist of olivine, orthopyroxene, and plagioclase. The groundmass with clear fluidal texture mainly contains fine grained plagioclase of < 0.1mm particle diameter, and also contains some pyroxene and opaque mineral.

090201-T: This sample (Gahinga V.), collected on the southern slope of Mt. Gahinga, is basalt. The phenocrysts consist of orthopyroxene, plagioclase, and olivine. The groundmass mainly contains plagioclase of <0.2mm particle diameter, with traces of orthopyroxene, olivine, and opaque mineral. Noticeable alteration is not recognized in the phenocrysts and groundmass.

2) K-Ar rock dating

The result of K-Ar rock dating of samples collected in the geological survey is shown in Table3-5.2. K-Ar rock dating of 5 samples collected in the geological survey was conducted to understand the volcanic history of Kinigi field and to evaluate the role of volcanism as a heat source in the geothermal conceptual model. The results of dating are shown in Table 3-5.2. The oldest sample is 083002-D (1.6±0.1Ma) from Sabyinyo V. 1, and the K-Ar dates of the other samples range from 1.0 to 0.7Ma.

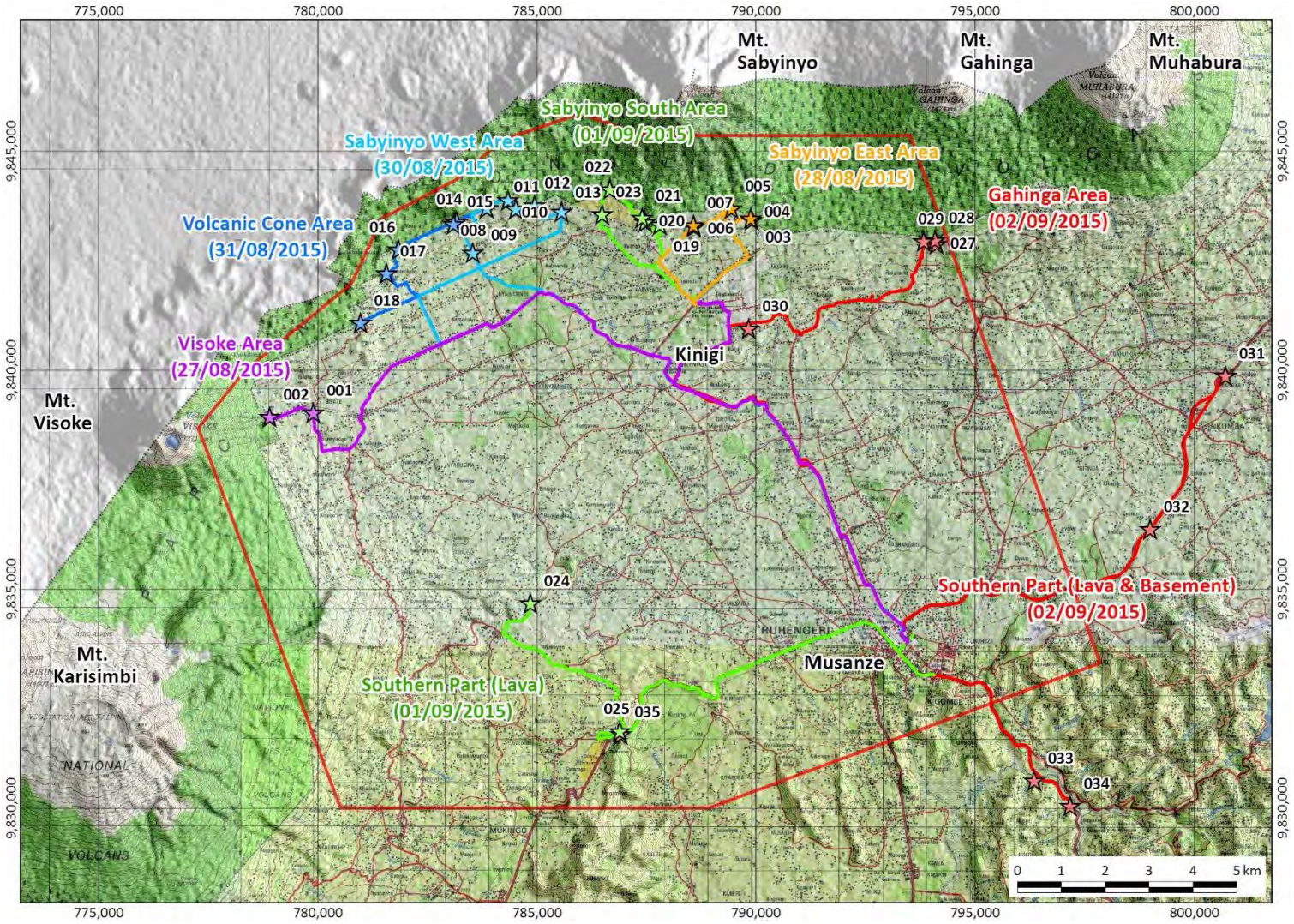

Source: JICA study team

Fig. 3-5.6 Location map of geological survey points in Kinigi field

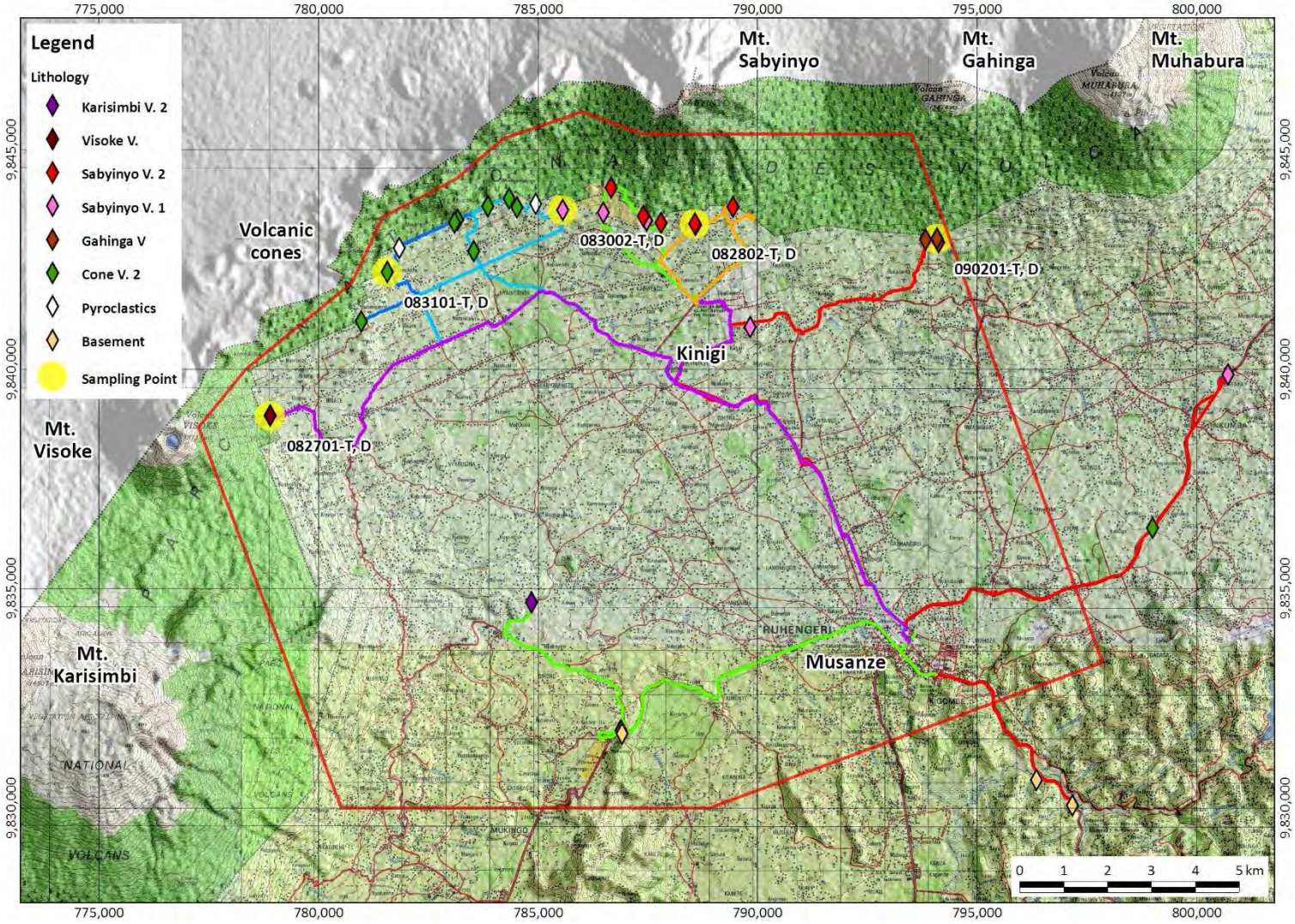

Source: JICA study team

Fig. 3-5.7 Result of geological survey in Kinigi field

Table 3-5.1 Results of petrographic observation

Ser. No.	Sample No.	District	Coordination*		Rock Name	Texture	Phenocryst**									Groundmass**								
			X	Y			Qtz	Pl	Leu	Bt	Hb	Cpx	Opx	Ol	Opq	Qtz	Pl	Bt	Hb	Cpx	Opx	Ol	Gl	Opq
1	082701-T	Mt. Visoke	778,902	9,838,942	Leucite - Clinopyroxene Andesite	Porphyritic (Intersertal)			◎			○	+		+		○			○				+
2	082802-T	Mt. Sabyinyo	788,582	9,843,317	Biotite Andesite	Porphyritic (Intergranular)		○		△		+	+		+		◎	+		+				+
3	083002-T	Mt. Sabyinyo	785,571	9,843,620	Olivine - Clinopyroxene Basalt	Porphyritic (Intergranular)		○				△		○	△		◎			○		+		
4	083101-T	Volcanic Cones	781,573	9,842,210	Olivine Basalt	Porphyritic (Intersertal)		+				+		△			◎			△				△
5	090201-T	Mt. Gahinga	794,103	9,842,969	Clinopyroxene - Olivine Basalt	Porphyritic (Intergranular)		△				○		△			◎			+		+		△

* Projection: Universal Transverse Mercator, Zone: 35S, Datum: WGS 1984, Spheroid: WGS 1984

** Qtz: Quartz, Pl: Plagioclase, Leu: Leucite, Bt: Biotite, Hb: Hornblende, Cpx: Clinopyroxene, Opx: Orthopyroxene, Ol: Olivine, Gl: Volcanic Glass, Opq: Opaque Mineral

◎: abundant (> 30 vol.%)
○: common (10 - 30 vol.%)
△ a little (3 - 10 vol.%)
+: rare (< 3 vol.%)

Source: JICA study team

Table 3-5.2 Results of K-Ar rock dating

Ser. No.	Sample No.	District	Coordination*		Rock Name (from petrographic observation)	K content (wt.%)	Rad. ^{40}Ar	Non Rad. ^{40}Ar (%)	K-Ar age (Ma)
			X	Y					
1	082701-D	Mt. Visoke	778,902	9,838,942	Leu - Cpx Andesite	2.35 2.41	0.093 0.095	96.8 94.4	1.0±0.4
2	082802-D	Mt. Sabyinyo	788,582	9,843,317	Bt Andesite	1.89 1.93	0.076 0.073	95.8 96.1	1.0±0.5
3	083002-D	Mt. Sabyinyo	785,571	9,843,620	Ol - Cpx Basalt	2.13 2.08	0.135 0.132	94.1 94.3	1.6±0.1
4	083101-D	Volcanic Cones	781,573	9,842,210	Ol Basalt	3.01 2.98	0.089 0.091	95.3 95.5	0.7±0.4
5	090201-D	Mt. Gahinga	794,103	9,842,969	Cpx - Ol Basalt	4.01 3.58	0.133 0.128	94.3 93.8	0.9±0.4

Source: JICA study team

(3) **Geology**

1) Stratigraphy

The Kinigi field is located in the northwestern part of Rwanda. The northern part of this field is situated in the Virunga Volcano Range (VVR) where there are some late Quaternary volcanoes. The southern part of this field is in the Butare Horst composed of Proterozoic mylonitised granitic and phyllitic complexes. Kinigi field is geologically composed of the Proterozoic mylonitised granitic and phyllitic complexes as a basement rock of young volcanoes, Cone volcanics, Sabyinyo volcanics, Gahinga volcanics, Visoke volcanics Karisimbi volcanics, and overlying debris flow deposits. The geological map and geological cross section of this field are shown in Fig. 3-5.8 and Fig. 3-5.9 respectively.

i) Basement rock (Br)

The basement rocks are exposed in the southern part of the study area, and they are Proterozoic mylonitised granitic and phyllitic complexes. In this region, a fault system trending N-S to NW-SE is dominant.

ii) Cone volcanics (Cv1 and Cv2)

Many basaltic cones occur between Karisimbi volcano and Sabyinyo volcano nearby in the D. R. Congo. They are mostly composed of basaltic scoria, pyroclastics and lava. Based on geographical characteristics, this unit was divided into Cv1 of lava flow and Cv2 of volcanic cones. Basalt lava is olivine basalt and is exposed in the southern part of the basement distributed area (Cv1).

iii) Sabyinyo volcanics (Sv1 and Sv2)

Sabyinyo volcano is situated in the north-central part of Kinigi field. The crater is located at the summit, and a collapse has given the summit the appearance of teeth. Sabyinyo volcanics are divided into two stages of volcanism. Basaltic lavas erupted in the first stage of volcanic activity (Sv1), and then andesitic lavas erupted in the second stage (Sv2). Andesite is characterized by inclusion of phenocrysts of biotite.

iv) Gahinga volcanics (Gv)

Gahinga volcano is a stratovolcano situated east of Sabyinyo volcano in the north-central part of Kinigi field. The volcanic rocks consist of olivine basalt overlying Sabyinyo basalt (Sv1).

v) Visoke volcanics (Vv)

Visoke volcano, situated at the eastern foot of Karisimbi volcano, is estimated to have erupted ahead of the Karisimbi volcano. Visoke volcanics consist of andesite containing phenocrysts of leucite.

vi) Karisimbi volcanics (Kv)

Karisimbi volcano is situated in the western part of Kinigi field. The volcanic rocks are alkaline basalt and pyroclastics which are divided into a lower member (Kv1) and an upper member (Kv2) based upon topographic characteristics. According to a previous study, the volcanic activity ranged from 0.01-0.24Ma

(Mulder, 1985).

vii) Debris flow deposits (Df)

Debris flow deposits are distributed in the southern part of Sabyinyo volcano. The deposits are composed of sand and gravel, which is mainly basalt (Sv1) and andesite (Sv2) of Sabyinyo volcanics.

2) Volcanic activity

The stratigraphy of Kinigi field is shown in Fig. 3-5.10. This field is situated in Virunga Volcano Range (VVR) where there are some late Quaternary volcanoes. It is estimated that volcanic activity in this field started with eruptions of Cone volcanics (the 1st stage, before 1.6Ma). They are mostly composed of basaltic cinder cone and basalt lava. A number of cone volcanos, which are situated in the northern part, extend in a NE-SW direction, and it is presumed that a basaltic dyke has intruded at a shallow depth. In the northeastern part of this field, Mt. Sabyinyo, Mt. Gahinga and Mt. Muhabura are arranged along an E-W axis. Sabyinyo volcanics are divided into two stages of volcanism. Basaltic lavas erupted in the first stage of volcanic activity occurred around 1.6Ma (Sv1), followed by andesitic lavas in the second stage at 1.0Ma- 0.5Ma (Sv2). At the same time, the basaltic Gahinga stratovolcano was active (after 1.0Ma). Mt. Visoke was also active after 1.0 Ma., followed by Mt. Karisimbi, which was active after 0.24 Ma.

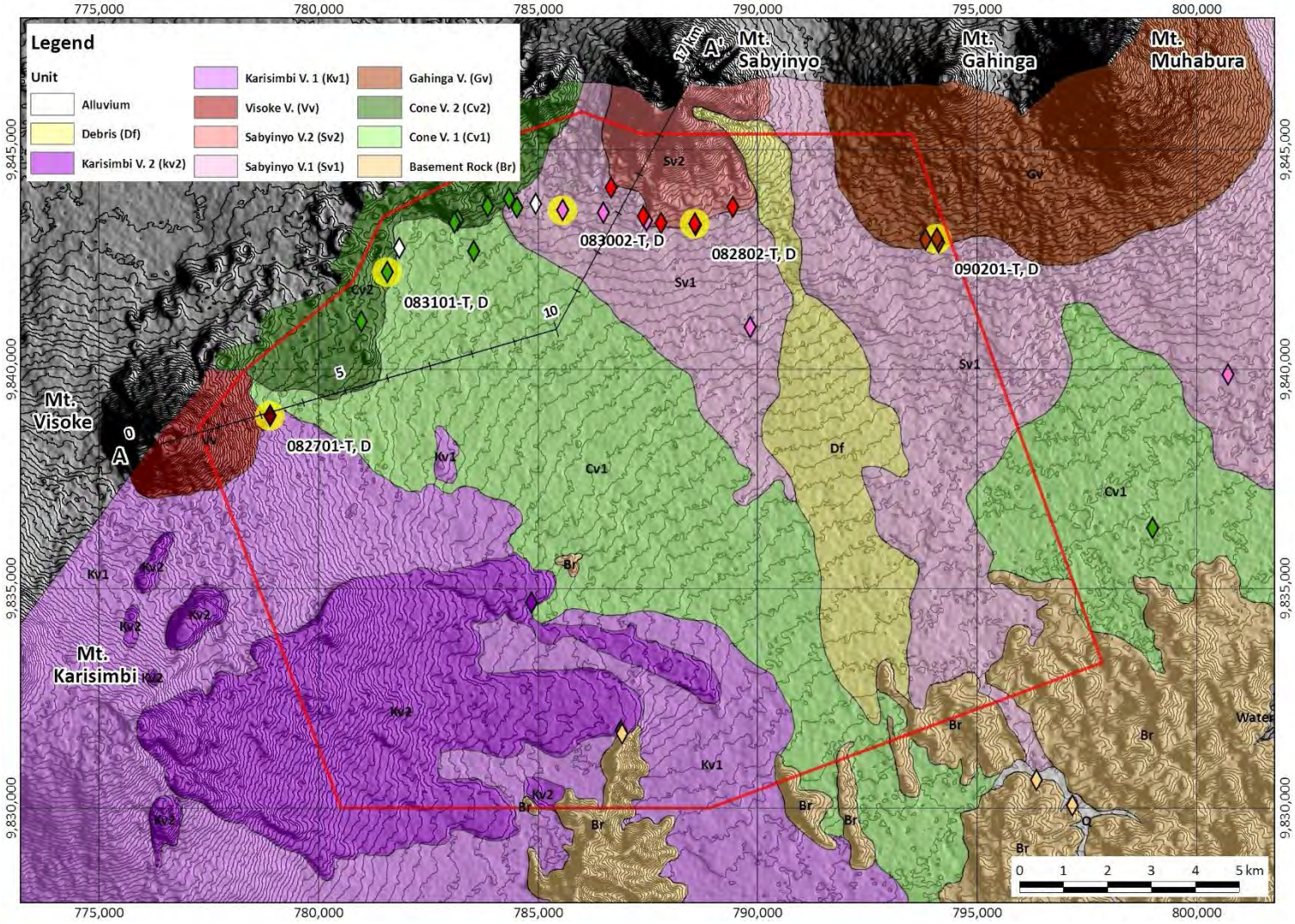

Source: JICA study team

Fig. 3-5.8 Geological map of Kinigi field

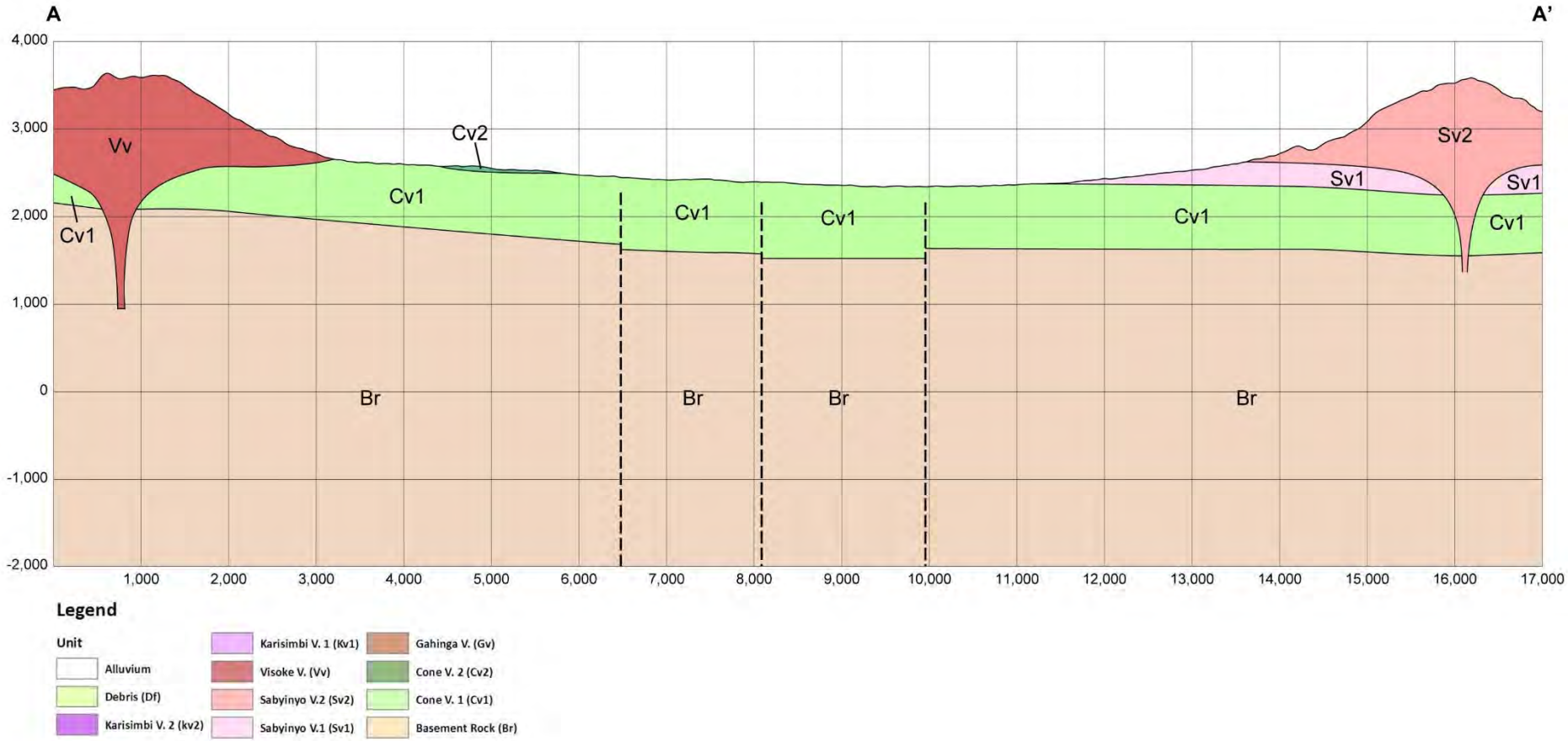

Source: JICA study team

Fig. 3-5.9 Geological cross section of Kinigi field

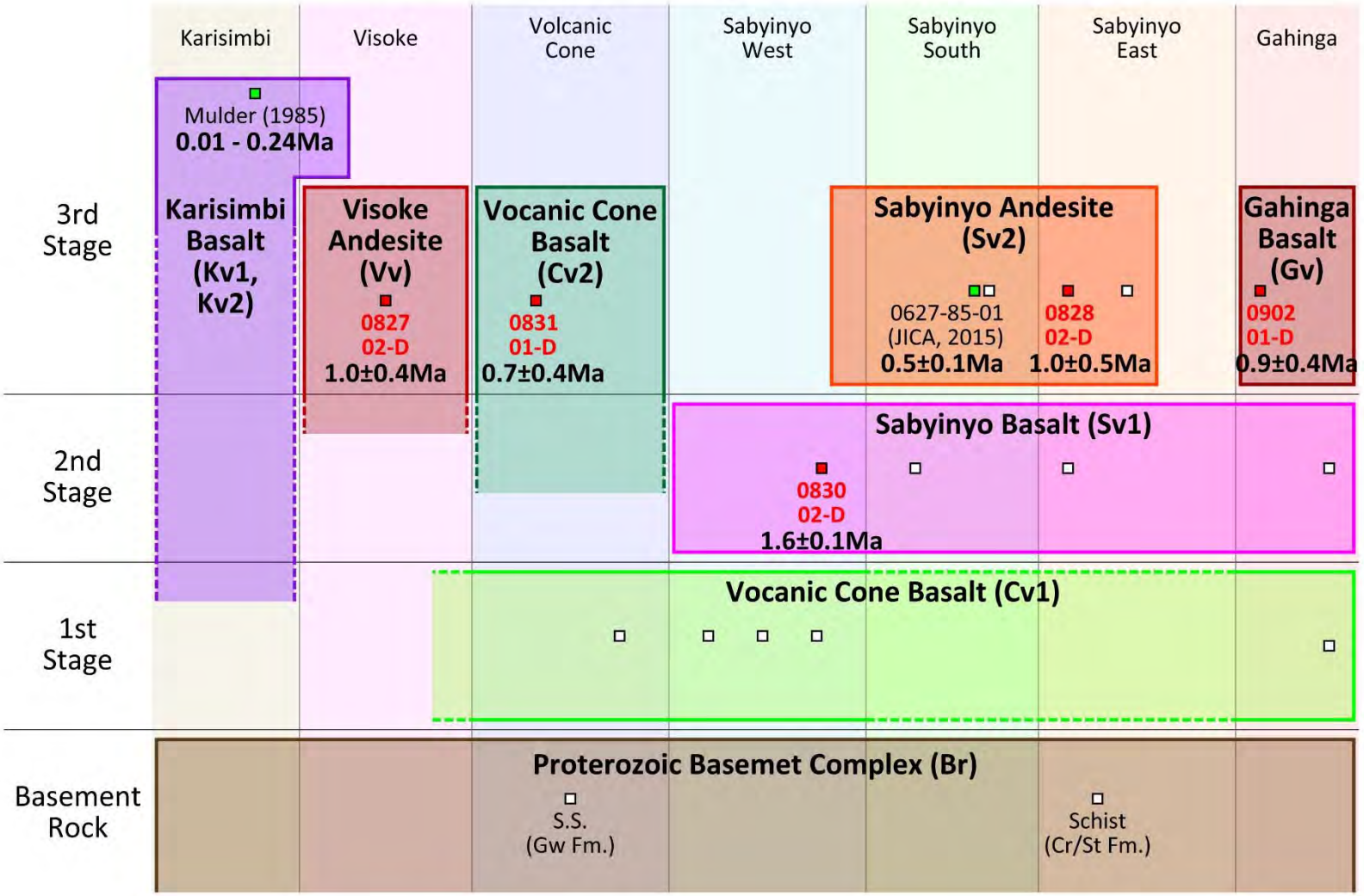

Source: JICA study team

Fig. 3-5.10 Stratigraphy of Kinigi field

(4) Technical transfer of geological survey techniques

Technology transfer related to geological survey techniques, was carried out as shown in Photo 3-5.1

No.1 Geological Survey Capacity Building

- ✓ Performed place: Kigari REG office
- ✓ Performed date: August 25, 2015
- ✓ Purpose: Outline of Capacity Building, overview of geological survey techniques and the remote sensing technology
- ✓ Participants: Jean Pascal NIYIGENA (Geochemist), Eugene KARANGWA (Reservoir engineer), Theoneste NZAYISENGA (Drilling engineer)

No.2 Hydrogeology (Geochemistry) Capacity Building

- ✓ Performed place: Kinigi
- ✓ Performed date: August 29, 2015
- ✓ Purpose: Understanding the hydrogeology (geochemistry) of Kinigi field
- ✓ Participants: Jean Pascal NIYIGENA (Geochemist), Eugene KARANGWA (Reservoir engineer)

No.3 Remote Sensing Analysis Capacity Building

- ✓ Performed place: Kinigi
- ✓ Performed date: August 29, 2015
- ✓ Purpose: Understanding the remote sensing analysis of Kinigi field
- ✓ Participants: Jean Pascal NIYIGENA (Geochemist), Eugene KARANGWA (Reservoir engineer)


Photo 3-5.1 Conditions for technical transfer of geological survey techniques

3.5.2. Gravity survey in Kinigi

(1) Field work for data acquisition

1) Time schedule of the field survey

The time schedule of the field survey for acquiring gravity data in the Kinigi field is shown in Table 3-5.3.

Table 3-5.3 Time schedule of field survey

Activity \ Date	August										September								October							
	22	23	24	25	26	27	28	29	30	31	1~22					23	24	25	26	27	28	29	30	1	2	3	4	5	6	7
1. Transfer（Japan→Kigali）																														
2. Preparation of survey Meeting with REG																														
3. Transfer（Kigali→Kinigi）																														
4. Check base site of GPS and main access road											September 1~22 Gravity measurent																			
5. Gravity measurement																														
6. Transfer(KinigiKigali) Transportation procedured of equipment																														
7. Preparation of capacity building Data processing																														
8. Capacity building																														
9. Preparation of field survey report Data processing																														
10. Reporting to JICA																														
11. Transfer（Kigali→Japan）																														

Source: JICA study team

2) Equipment utilized for the gravity data acquisition

i) Gravimeter

In this gravity survey, gravity differences between a reference station and actual survey stations were measured using relative gravimeters.

The relative gravimeters used in the survey were a CG-5 gravimeter manufactured by CANADA SCINTREX and a D-type gravimeter manufactured by LaCoste & Romberg as a backup gravimeter as shown in Fig. 3-5.11 and Fig. 3-5.12.

During the CG-5 measurements, statistical data processing using 720 data samples was performed to improve the measurement accuracy (120 seconds of measurement was done with 6 data samples measured per second). This gravimeter is capable of storing the acquired data in internal memory, and thus it is easy to transfer and manage the data using a personal computer with a USB port. The specifications of the CG-5 gravimeter are shown in Table 3-5.4.

The value of the dynamic range of the LaCoste D-type gravimeter is 200 mGal. It is possible to conduct a gravity survey within 5 micro-gal standard field repeatability all over the world to reset its

range. The drift range of the gravimeter is below 1 mgal/month and it is tough and portable. so its advantage enable to utilize the gravimeter in gravity survey. The specifications of the D-type gravimeter are shown in Table 3-5.5.

Source: JICA study team

Fig. 3-5.11 CG-5 Gravimeter

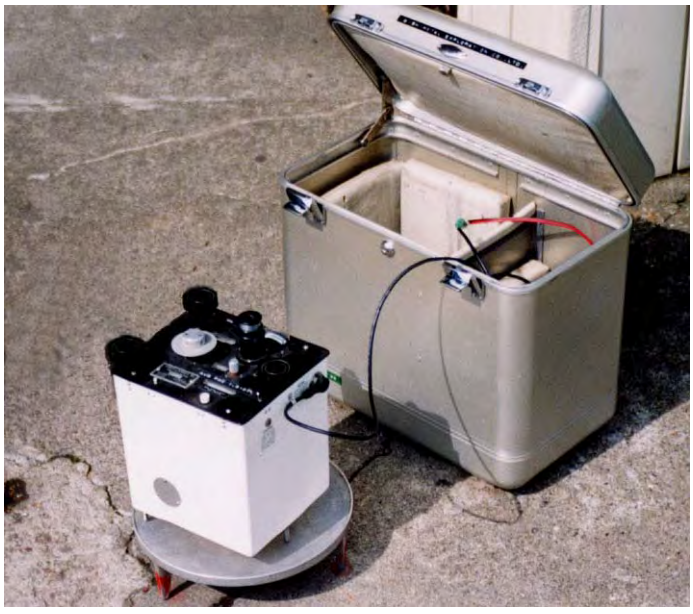

Source: JICA study team

Fig. 3-5.12 D-type Gravimeter

Table 3-5.4 Table of specifications of CG-5

Sensor type	Fused Quartz using electrostatic nulling
Reading resolution	1 micro Gal
Standard Field Repeatability	<5 micro Gal
Automated Corrections	Tidal correction, terrain correction, temperature correction, drift correction
Data output	RS-232C, USB interface
Dimensions	21cm×22cm×31cm
Weight (including battery)	8kg

Source: JICA study team

Table 3-5.5 Table of specifications of D type gravimeter

Sensor type	Elastic invariable zero-length spring
Standard field repeatability	±5 micro Gal
Drift range	<1mGal／month
Dynamic range	200mGal
Method of displacement detection	×70 microscope
Dimensions	18cm×18cm×25cm
weight	8kg

Source: JICA study team

ii) GPS receiver

A GPS receiver is a device used for measuring position information (latitude, longitude, altitude) at a measurement point. It is necessary to perform various corrections of gravity value in order to calculate the Bouguer anomaly data. The corrections of gravity value require latitude, longitude and altitude information. Two types of GPS receivers, TOPCON's GRS-1 and 2 sets of TRIMBLE's 5700 L1 were used in this survey. The receivers are shown in Table 3-5.6. The GRS-1 uses two-frequencies, while the 5700 L1 uses one frequency in order to acquire position information. These devices are composed of an antenna, a controller and a receiver. The antenna is to receive a signal from GPS satellites which are located at an altitude of around 20,000 km. The receiver is composed of a CPU and an internal ROM program for calculating the location of the receiver. The controller consists of a small computer equipped with Windows Mobile, which is used for setting the measurement parameters (station name, antenna height, measurement method, observation time, etc.) of the survey station. A GPS receiver is shown in Fig. 3-5.13

Table 3-5.6 GPS receiver specifications

Name	GRS-1	5700 L1
Receiver wave	Code L1 L2 C/A P（2-frequency）	Code L1 C/A（1-frequency）
Accuracy（Static）	Horizontal： ±（3mm+0.5ppm×baseline length km）	Horizontal： ±（5mm+0.5ppm×baseline length km）
	Vertical： ±（5mm+0.5ppm×baseline length km）	Vertical： ±（5mm+1.0ppm×baseline length km）
Dimensions	215mm×93mm×53mm （Main body of receiver）	135mm×85mm×240mm （Main body of receiver）
Weight	0.77kg	1.4 kg
	（Including battery）	（Including battery）
Software for data analysis	GNSS Pro Ver.7.52 (TOPCON), Trimble Total Control™ (TRIMBLE)	
Interval sampling	30 second (short static)	
Data acquisition time	30 minutes/ 1 measurement station (short static)	
Ephemeris	Broadcast Ephemeris	

Source: JICA study team

Source: JICA study team

Fig. 3-5.13 GPS receiver

3) Measurement method

i) Gravity measurement at each station

In this gravity survey, only the CG-5 gravimeter was used. The gravity value at each station was determined by the difference between the measured data at each station and the measured data at the reference station, using the relative gravimeter. During the measurement at each station, 720 gravity data samples were acquired in 120 seconds (6 data samples were measured per second). If the standard deviation of the acquired data was large, re-measurement was conducted until satisfactory data was obtained. It should be noted that the gravity measurement was conducted after confirming that the gravimeter tripod was steady.

ii) Survey of each measurement point

In this survey, the electronic reference point was located far from the survey area and was not suitable as a reference station for the survey. As a result, we installed a GPS receiver at a base station and this station was used as a reference point during the survey period. Since the coordinates of the reference station were unknown, we carried out a coordinate survey for 3 days. After installing the 5700 L1 at the reference station, measurement at each of the other stations using the GRS-1 and 5700 L1 were performed. The duration for the observation at each measurement station was approximately 30 minutes. GPS (GNSS) data processing was done using data processing software developed by

TOPCON Inc. The two types of software used were GNSS integrated data processing program (GNSS-Pro ver 7.52) and Trimble Total Control™ developed by TRIMBLE Company. After calculating the baseline between the 5700 L1 and the reference point (the 3D vector between the two points), the position of the reference point was precisely obtained. In addition, since the height of the GPS survey station was determined from the ellipsoid, and the height differs from altitude, a deduction of the ellipsoid height from the geoid height must be done to obtain an altitude conversion. In this survey, the heights of the measurement stations were calculated from the height data obtained by GPS, then integrated data processing was performed using Trimble Total Control™.

The latitude, longitude and altitude of each station were determined by performing the above-mentioned process. The results of the GPS measurements are shown in Table 3-5.7, while the location of each station is shown in Fig. 3-5.14. Stations with an “R” postfixed at the end of the name are stations at which remeasurement was necessary.

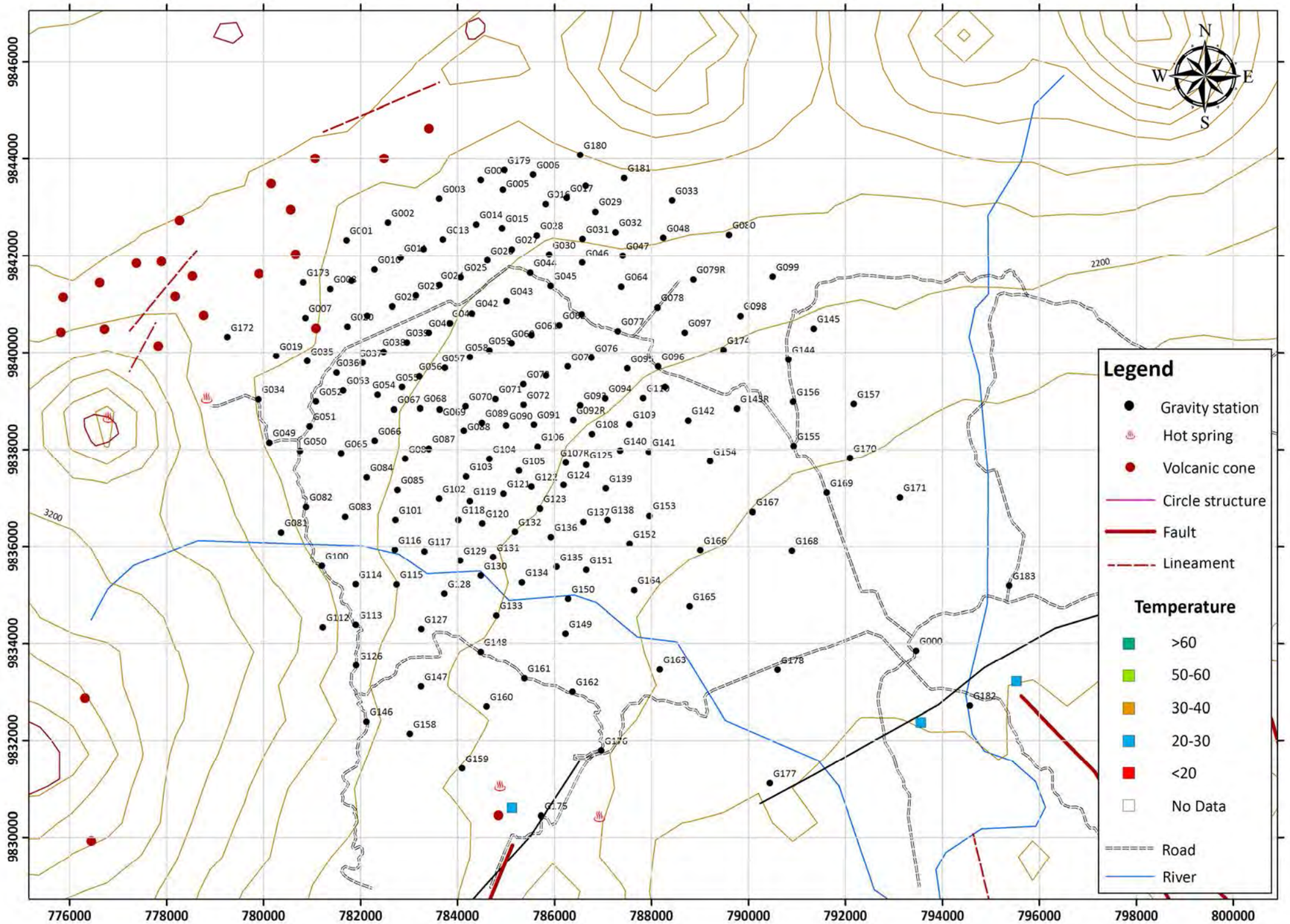

Source: JICA study team

Fig. 3-5.14 Location of gravity stations

Table 3-5.7 Results of GPS measurement (1)

Station	WGS84						UTM		Elevation (m)
	Latitude			Longitude			NS(m)	EW(m)	
	Deg	Min	Sec	Deg	Min	Sec			
G000	-1	30	5.838	29	38	13.926	9833848	793459	1837.86
G001	-1	25	30.468	29	31	53.682	9842325	781707	2540.20
G002	-1	25	18.618	29	32	21.384	9842688	782564	2501.82
G003	-1	25	2.688	29	32	55.524	9843177	783621	2499.42
G004	-1	24	50.160	29	33	23.220	9843561	784478	2501.21
G005	-1	24	56.694	29	33	37.872	9843360	784931	2499.44
G006	-1	24	46.500	29	33	58.128	9843672	785558	2515.07
G007	-1	26	22.896	29	31	26.322	9840715	780859	2624.00
G008	-1	26	3.492	29	31	42.816	9841311	781370	2579.34
G009	-1	25	57.828	29	31	57.030	9841484	781810	2536.17
G010	-1	25	50.280	29	32	12.414	9841716	782286	2503.65
G011	-1	25	42.198	29	32	29.856	9841963	782825	2480.31
G012	-1	25	36.384	29	32	45.048	9842142	783295	2462.39
G013	-1	25	29.910	29	32	57.894	9842340	783693	2455.90
G014	-1	25	19.806	29	33	20.232	9842650	784384	2445.19
G015	-1	25	22.242	29	33	37.452	9842574	784917	2431.86
G016	-1	25	6.210	29	34	6.534	9843066	785817	2451.78
G017	-1	25	2.034	29	34	20.574	9843194	786251	2475.89
G018	-1	24	53.976	29	34	33.120	9843441	786640	2521.59
G019	-1	26	48.342	29	31	6.864	9839933	780256	2613.91
G020	-1	26	28.482	29	31	54.312	9840542	781724	2497.11
G021	-1	26	21.234	29	32	7.608	9840764	782136	2486.19
G022	-1	26	15.090	29	32	24.288	9840953	782652	2463.53
G023	-1	26	7.692	29	32	39.984	9841180	783138	2451.81
G024	-1	26	0.732	29	32	55.614	9841393	783621	2435.00
G025	-1	25	55.440	29	33	9.816	9841555	784061	2418.74
G026	-1	25	43.986	29	33	27.582	9841906	784611	2418.11
G027	-1	25	36.480	29	33	43.872	9842137	785115	2411.65
G028	-1	25	27.096	29	34	0.546	9842424	785631	2411.25
G029	-1	25	11.166	29	34	39.726	9842913	786844	2462.50

Source: JICA study team

Table 3-5.7 Results of GPS measurement (2)

Station	WGS84						UTM		Elevation (m)
	Latitude			Longitude			NS(m)	EW(m)	
	Deg	Min	Sec	Deg	Min	Sec			
G030	-1	25	40.092	29	34	8.820	9842025	785887	2383.53
G031	-1	25	29.382	29	34	31.152	9842353	786578	2404.87
G032	-1	25	24.828	29	34	53.130	9842492	787258	2433.00
G033	-1	25	3.738	29	35	30.750	9843139	788422	2474.23
G034	-1	27	17.532	29	30	55.116	9839037	779892	2585.64
G035	-1	26	51.798	29	31	27.672	9839827	780900	2575.53
G036	-1	26	59.574	29	31	47.058	9839587	781499	2481.30
G037	-1	26	52.764	29	32	4.632	9839796	782043	2456.39
G038	-1	26	45.468	29	32	18.600	9840019	782475	2433.74
G039	-1	26	39.114	29	32	34.152	9840214	782956	2433.13
G040	-1	26	32.640	29	32	48.582	9840412	783403	2411.56
G041	-1	26	26.148	29	33	2.784	9840612	783842	2400.65
G042	-1	26	19.524	29	33	17.322	9840815	784292	2379.65
G043	-1	26	11.394	29	33	40.608	9841064	785013	2369.35
G044	-1	25	52.314	29	33	56.250	9841650	785497	2370.94
G045	-1	26	1.206	29	34	9.756	9841376	785915	2343.44
G046	-1	25	45.450	29	34	30.906	9841859	786570	2359.66
G047	-1	25	40.650	29	34	57.948	9842006	787406	2383.66
G048	-1	25	28.554	29	35	24.924	9842377	788241	2398.62
G049	-1	27	46.500	29	31	2.430	9838146	780117	2575.94
G050	-1	27	52.050	29	31	22.878	9837975	780749	2522.76
G051	-1	27	35.418	29	31	29.232	9838486	780946	2519.49
G052	-1	27	19.014	29	31	33.408	9838990	781076	2504.89
G053	-1	27	11.538	29	31	51.510	9839219	781636	2465.06
G054	-1	27	14.412	29	32	14.508	9839130	782348	2428.89
G055	-1	27	9.234	29	32	30.876	9839288	782854	2404.34
G056	-1	27	2.052	29	32	42.276	9839509	783207	2405.90
G057	-1	26	56.214	29	32	59.436	9839688	783738	2384.60
G058	-1	26	48.858	29	33	16.056	9839913	784252	2365.71
G059	-1	26	44.376	29	33	29.094	9840050	784656	2348.36

Source: JICA study team

Table 3-5.7 Results of GPS measurement (3)

Station	WGS84						UTM		Elevation (m)
	Latitude			Longitude			NS(m)	EW(m)	
	Deg	Min	Sec	Deg	Min	Sec			
G060	-1	26	39.504	29	33	43.914	9840200	785114	2334.06
G061	-1	26	34.050	29	33	57.066	9840367	785521	2327.95
G062	-1	26	27.378	29	34	15.630	9840571	786096	2311.85
G063	-1	26	20.082	29	34	30.498	9840795	786556	2309.39
G064	-1	26	1.680	29	34	57.000	9841360	787376	2324.71
G065	-1	27	53.706	29	31	50.310	9837923	781598	2474.04
G066	-1	27	45.120	29	32	12.744	9838186	782292	2420.96
G067	-1	27	24.216	29	32	25.560	9838828	782689	2409.52
G068	-1	27	23.436	29	32	42.936	9838852	783226	2376.65
G069	-1	27	24.258	29	32	55.884	9838826	783627	2358.79
G070	-1	27	22.152	29	33	13.290	9838890	784165	2326.33
G071	-1	27	17.166	29	33	33.108	9839042	784779	2297.60
G072	-1	27	21.168	29	33	51.846	9838919	785358	2265.11
G073	-1	27	7.146	29	33	51.738	9839350	785355	2286.84
G074	-1	27	1.308	29	34	6.894	9839529	785824	2276.86
G075	-1	26	55.236	29	34	21.426	9839715	786274	2267.18
G076	-1	26	49.278	29	34	37.110	9839897	786759	2256.27
G077	-1	26	31.434	29	34	54.672	9840445	787303	2267.37
G078	-1	26	15.546	29	35	21.114	9840933	788121	2284.35
G079	-1	25	53.778	29	35	36.882	9841601	788610	2322.45
G079R	-1	25	56.838	29	35	45.144	9841507	788865	2311.93
G080	-1	25	26.484	29	36	8.886	9842439	789601	2389.42
G081	-1	28	46.878	29	31	10.308	9836290	780359	2643.23
G082	-1	28	29.808	29	31	26.970	9836814	780875	2554.80
G083	-1	28	36.174	29	31	52.998	9836618	781679	2463.60
G084	-1	28	9.948	29	32	7.320	9837423	782123	2428.97
G085	-1	28	18.402	29	32	27.876	9837163	782759	2368.90
G086	-1	27	57.294	29	32	33.066	9837811	782920	2405.56
G087	-1	27	50.406	29	32	48.714	9838022	783404	2355.99
G088	-1	27	38.322	29	33	12.078	9838393	784127	2318.07

Source: JICA study team

Table 3-5.7 Results of GPS measurement (4)

Station	WGS84						UTM		Elevation (m)
	Latitude			Longitude			NS(m)	EW(m)	
	Deg	Min	Sec	Deg	Min	Sec			
G089	-1	27	33.126	29	33	24.132	9838552	784500	2300.72
G090	-1	27	34.800	29	33	40.284	9838500	785000	2267.14
G091	-1	27	34.104	29	33	58.764	9838521	785572	2246.00
G092	-1	27	34.992	29	34	16.224	9838493	786112	2216.28
G092R	-1	27	31.122	29	34	25.152	9838612	786388	2209.58
G093	-1	27	21.498	29	34	29.628	9838907	786527	2219.77
G094	-1	27	16.764	29	34	46.296	9839052	787042	2207.17
G095	-1	26	56.526	29	35	1.062	9839674	787500	2214.40
G096	-1	26	55.128	29	35	21.600	9839716	788135	2201.12
G097	-1	26	32.334	29	35	39.420	9840416	788687	2237.28
G098	-1	26	21.054	29	36	16.446	9840761	789833	2257.75
G099	-1	25	54.918	29	36	38.046	9841564	790502	2283.10
G100	-1	29	9.402	29	31	37.542	9835597	781200	2566.19
G101	-1	28	38.358	29	32	26.484	9836550	782715	2361.37
G102	-1	28	24.270	29	32	55.752	9836981	783621	2302.62
G103	-1	28	9.312	29	33	13.644	9837441	784175	2286.07
G104	-1	27	57.288	29	33	29.100	9837810	784653	2278.37
G105	-1	28	5.262	29	33	48.834	9837564	785263	2235.45
G106	-1	27	49.014	29	34	1.428	9838063	785653	2225.35
G107	-1	27	48.330	29	34	16.566	9838083	786122	2199.12
G107R	-1	27	59.730	29	34	20.148	9837733	786232	2187.79
G108	-1	27	40.464	29	34	37.578	9838324	786772	2190.12
G109	-1	27	33.954	29	35	2.478	9838523	787542	2169.91
G110	-1	27	16.488	29	35	11.616	9839060	787826	2181.63
G111	-1	27	8.988	29	35	26.190	9839290	788277	2179.92
G112	-1	29	50.406	29	31	38.160	9834337	781218	2675.01
G113	-1	29	48.828	29	32	0.234	9834385	781901	2510.72
G114	-1	29	21.780	29	32	0.072	9835216	781897	2494.84
G115	-1	29	21.834	29	32	27.354	9835213	782740	2390.61
G116	-1	28	58.398	29	32	26.250	9835934	782707	2354.35

Source: JICA study team

Table 3-5.7 Results of GPS measurement (5)

Station	WGS84						UTM		Elevation (m)
	Latitude			Longitude			NS(m)	EW(m)	
	Deg	Min	Sec	Deg	Min	Sec			
G117	-1	28	59.454	29	32	45.906	9835900	783315	2284.95
G118	-1	28	38.220	29	33	8.520	9836552	784015	2278.94
G119	-1	28	25.860	29	33	16.212	9836932	784254	2267.40
G120	-1	28	40.578	29	33	24.450	9836479	784508	2250.45
G121	-1	28	20.790	29	33	38.670	9837087	784948	2239.68
G122	-1	28	16.104	29	33	57.240	9837230	785523	2211.45
G123	-1	28	30.780	29	34	2.988	9836779	785700	2194.50
G124	-1	28	14.808	29	34	18.642	9837269	786185	2185.29
G125	-1	28	1.290	29	34	33.702	9837684	786651	2173.91
G126	-1	30	16.134	29	32	0.486	9833545	781907	2473.90
G127	-1	29	51.624	29	32	43.794	9834297	783248	2309.76
G128	-1	29	28.038	29	32	59.124	9835022	783723	2322.66
G129	-1	29	5.592	29	33	9.726	9835711	784052	2240.17
G130	-1	29	15.870	29	33	23.412	9835395	784474	2261.11
G131	-1	29	3.408	29	33	31.776	9835777	784734	2202.91
G132	-1	28	46.146	29	33	46.254	9836307	785182	2182.95
G133	-1	29	42.522	29	33	33.846	9834575	784796	2178.08
G134	-1	29	20.436	29	33	50.874	9835253	785324	2152.58
G135	-1	29	9.906	29	34	14.094	9835576	786042	2098.40
G136	-1	28	49.686	29	34	10.242	9836198	785924	2164.31
G137	-1	28	39.486	29	34	31.920	9836510	786595	2146.38
G138	-1	28	38.112	29	34	48.018	9836552	787093	2096.22
G139	-1	28	17.220	29	34	46.866	9837194	787058	2129.71
G140	-1	27	51.744	29	34	56.352	9837977	787352	2140.53
G141	-1	27	52.512	29	35	15.486	9837953	787944	2124.05
G142	-1	27	31.302	29	35	41.778	9838603	788758	2135.27
G143	-1	27	23.652	29	36	13.626	9838837	789743	2082.78
G143R	-1	27	23.490	29	36	14.262	9838842	789763	2082.08
G144	-1	26	50.388	29	36	48.498	9839859	790823	2139.40
G145	-1	26	29.484	29	37	5.316	9840500	791344	2177.86

Source: JICA study team

Table 3-5.7 Results of GPS measurement (6)

Station	WGS84						UTM		Elevation (m)
	Latitude			Longitude			NS(m)	EW(m)	
	Deg	Min	Sec	Deg	Min	Sec			
G146	-1	30	53.820	29	32	7.362	9832387	782119	2440.280
G147	-1	30	30.378	29	32	43.806	9833106	783247	2261.513
G148	-1	30	6.894	29	33	23.472	9833826	784475	2177.463
G149	-1	29	54.636	29	34	20.010	9834201	786224	2069.585
G150	-1	29	31.446	29	34	21.768	9834914	786279	2066.342
G151	-1	29	11.838	29	34	33.912	9835516	786655	2079.871
G152	-1	28	54.186	29	35	2.808	9836057	787550	2055.245
G153	-1	28	35.346	29	35	15.924	9836636	787956	2056.198
G154	-1	27	58.746	29	35	56.262	9837759	789205	2077.166
G155	-1	27	48.414	29	36	52.146	9838075	790934	2022.877
G156	-1	27	18.804	29	36	51.666	9838985	790920	2078.955
G157	-1	27	20.322	29	37	32.082	9838937	792170	2056.875
G158	-1	31	2.034	29	32	36.288	9832134	783013	2281.103
G159	-1	31	25.308	29	33	11.286	9831417	784095	2189.748
G160	-1	30	43.860	29	33	27.462	9832690	784597	2186.249
G161	-1	30	24.810	29	33	52.626	9833275	785376	2121.128
G162	-1	30	33.882	29	34	24.666	9832995	786366	2078.385
G163	-1	30	18.714	29	35	22.986	9833459	788171	1999.233
G164	-1	29	25.542	29	35	5.922	9835094	787645	2017.577
G165	-1	29	36.348	29	35	42.756	9834760	788784	1950.178
G166	-1	28	58.374	29	35	49.968	9835927	789008	1998.189
G167	-1	28	32.778	29	36	24.666	9836712	790082	1984.112
G168	-1	28	58.584	29	36	51.096	9835918	790899	1938.866
G169	-1	28	19.884	29	37	14.142	9837107	791613	1967.792
G170	-1	27	56.436	29	37	29.604	9837827	792092	1997.336
G171	-1	28	22.992	29	38	3.018	9837010	793125	1933.580
G172	-1	26	35.682	29	30	34.302	9840324	779249	2671.897
G173	-1	25	59.034	29	31	24.912	9841448	780816	2621.691
G174	-1	26	44.088	29	36	5.292	9840054	789487	2187.367
G175	-1	31	57.036	29	34	3.900	9830440	785721	2107.059

Source: JICA study team

Table 3-5.7 Results of GPS measurement (7)

Station	WGS84						UTM		Elevation (m)
	Latitude			Longitude			NS(m)	EW(m)	
	Deg	Min	Sec	Deg	Min	Sec			
G176	-1	31	13.038	29	34	43.884	9831791	786959	2070.98
G177	-1	31	35.118	29	36	36.486	9831108	790441	1795.30
G178	-1	30	18.936	29	36	41.538	9833449	790600	1875.52
G179	-1	24	43.428	29	33	38.838	9843767	784961	2527.13
G180	-1	24	32.976	29	34	29.460	9844087	786527	2591.55
G181	-1	24	48.618	29	34	58.896	9843605	787437	2568.16
G182	-1	30	42.780	29	38	49.722	9832711	794564	1833.92
G183	-1	29	22.224	29	39	15.870	9835186	795376	1870.43

Source: JICA study team

(2) **Data processing and analysis method**

1) Data processing

Some necessary corrections were applied to the acquired data at each station to calculate Bouguer anomaly values at each station. Fig.3-5.15 shows the procedure used to process the gravity data.

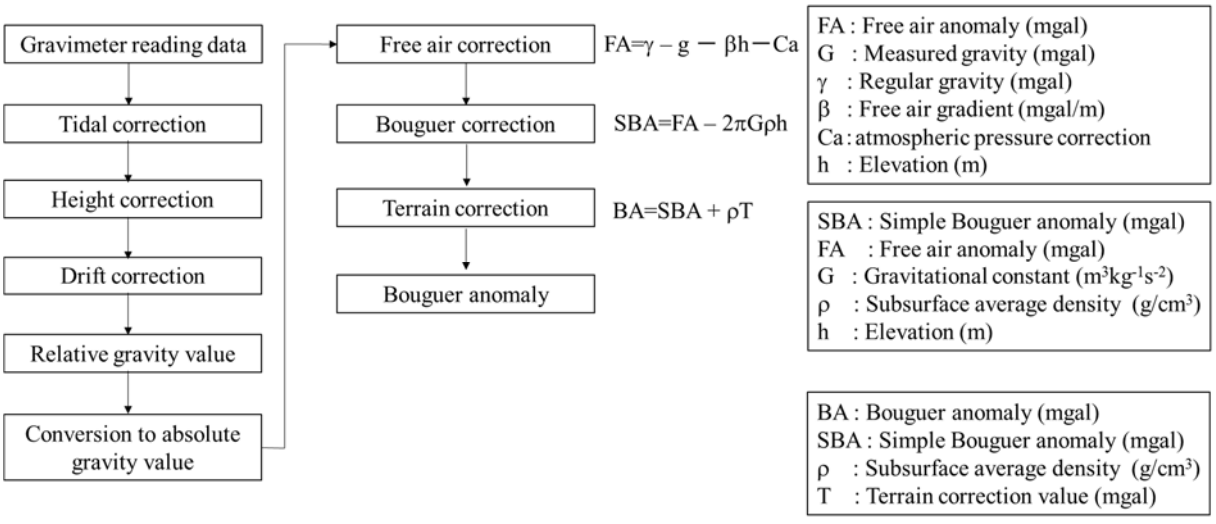

Source: JICA study team

Fig. 3-5.15 The data processing procedure

i) Tidal correction

A gravimeter is sensitive enough to record the gravity changes caused by the movements of the Sun and the Moon, which vary according to latitude and time. Tidal correction is conducted to eliminate the

influence of the attraction caused by the movement of the Sun and the Moon. In this survey the Scintrex CG-5 gravimeter was used. The Scintrex CG-5 utilizes an analytical program to correct automatically for tidal values, during gravity measurements.

ii) Height correction

Correction of gravimeter height from the ground surface is necessary since the gravity value decreases when the distance between the station and the datum surface increases. This is done using vertical gravity gradientheight correction (0.3086 mgal/m), which is expressed by the following equation:

$V_{hi} = 0.3086 \times Hi$

V_{hi} : height correction value（mgal）

Hi : the height of the gravimeter from the surface（m）

iii) Drift correction

The spring in the gravimeter extends by itself with time, and the measured gravity value is influenced by this extension of the spring. The error in gravity value caused by the extension of the spring length with time is called “drift”. When the spring length increases, the measured gravity value becomes larger than the value without drift. This gravity change caused by drift is corrected by drift correction. Errors caused by the rapid change of temperature and by impacts on the gravimeter during transport are also removed by the drift correction. In order to determine the level of drift, a base station for gravity measurement is established. Next, gravity measurements are taken at multiple locations, starting and ending at the base station. The gravity difference at the base station between start point and end point is regarded as the drift value because no gravity difference would occur at same station without drift effects. The drift value at each station is prorated depending on the elapsed time since the first measurement of the day occurred.

iv) Free air correction

Free air correction corrects for the influence caused by the difference between the measurement elevation and the geoid level. The vertical gravity gradient is not necessarily constant, but in this survey an average value of 0.3086 mgal/m was used. The equation is shown below:

$F = 0.3086 \times h$

F : free air correction value（mgal）

h : elevation of the stations （m）

v) Bouguer correction

The Bouguer correction accounts for the gravitational attraction of the material between the station and the datum plane that is ignored in the free air correction. The Bouguer correction is conducted by using the equation shown below. The estimated density is included in the equation. The method used to determine the estimated density is shown in a following section. In this survey, 2.64 g/cm^3 was used as the value of the estimated density.

$B = 2\pi G\rho h$

B : Bouguer correction value（mgal）

G : Gravitational constant（$6.67\times10^{-11}m^3kg^{-1}s^{-2}$）

ρ : Estimated density（g/cm^3）

H : Elevation of the stations（m）

vi) Terrain correction

Terrain correction is used to eliminate the influence of the undulation of terrain on the measured gravity value. In this survey, the effect of terrain within a 60 km radius centering on the measuring station was calculated by using the digital elevation data of the SRTM (Shuttle Radar Topography Mission). This circular range is divided into four zones depending on the distance from the measuring stations; extremely near zone (0~500m), near zone (500m~4km), medium zone (4~16km) and far zone (16~60km). The terrain correction value was calculated in each zone using the analytical program for terrain correction developed by Komazawa (1980)

vii) Calculation of the Bouguer anomaly

After calculating each correction, the Bouguer anomaly is formulated by the following equation:

$\Delta B = g_{obs} - \gamma + \beta h - 2\pi G\rho h + \rho T$

ΔB : Bouguer anomaly（mgal）

g_{obs} : Measured gravity value（mgal）

γ : Regular gravity （mgal）

β : Free air gradient（mgal/m）

h : Elevation（m）

G : Gravitational constant（$6.67\times10^{-11}m^3kg^{-1}s^{-2}$）

ρ : Estimated density（g/cm^3）

T : Terrain correction value（mgal）

2) Evaluation of the estimated density

There are various methods which can be used to estimate surface density such as directly measuring the density of core samples, comparing the distribution of the Bouguer anomaly with a topography map, the G-H and F-H correlation methods, etc. In this survey, G-H and F-H (Hagiwara,1978 ; Parasnis,1979) correlation methods were used to calculate the estimate density in Kinigi field. In G-H correlation method, h is correlated with $g_{obs}-\gamma+T$ (or $g_{obs}-\gamma$). In the F-H correlation method, F and H are ploted on the graph and the gradient of the approximate line is calculated.

Where,

$$F = g_{obs} - \gamma + \beta h + Ca$$

$$H = 2\pi Gh + T$$

The estimated density is calculated to minimize the residual between the Bouguer anomaly value at each station and the average Bouguer anomaly value of all stations. The gradient of the approximate line is the same as the estimated density. Figs. 3-5.16 and 3-5.17 show the G-H and F-H correlation map. The estimated density is 2.38 g/cm^3 using the G-H correlation method and 2.42 g/cm^3 using the F-H correlation method. The value of estimated density in Kinigi field is 2.40 g/cm^3, which is the average of the results of the two methods.

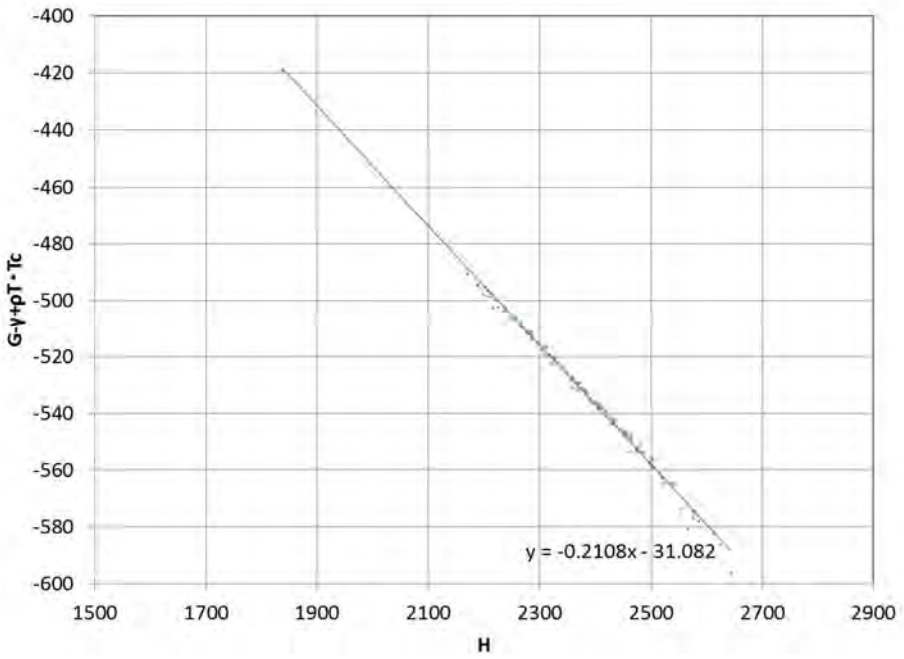

Source: JICA study team

Fig. 3-5.16 Results of G-H correlation method

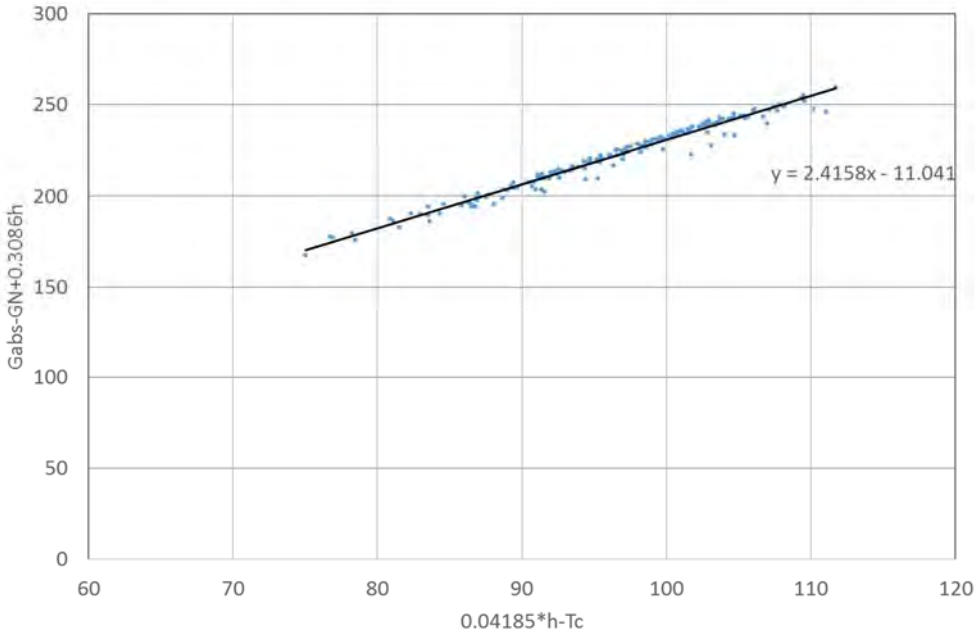

Source: JICA study team

Fig. 3-5.17 Results of F-H correlation method

3) Bouguer anomaly

The Bouguer anomaly, caused by the heterogeneous character of the density distribution in the subsurface, is calculated in data processing. The distribution of the subsurface density can be estimated from the Bouguer anomaly. The gravity value is the net force, both the centrifugal force caused by the Earth's rotation and the attracting force occurring between the Earth, the Sun and the Moon. The magnitude of the centrifugal force of the Earth's rotation is at its maximum at the equator and at its minimum at the poles, which causes the gravity value to vary based on latitude. In addition, the gravity value at higher elevations is lower because the attracting force of the Earth is smaller. The tidal force depends on the position of the stations relative to the Sun and the Moon, so the measured gravity changes with time at the measuring stations. The terrain effect is caused by the attracting force occurring near a body with large mass such as a mountain. Even if these corrections are conducted, the corrected gravity has different values at each of the stations. The difference between the corrected gravity and the average gravity is called the Bouguer anomaly. It is caused by the heterogeneous character of the density distribution in the subsurface and elucidating this is the purpose of the gravity survey.

4) Trend surface analysis

The objective of trend surface analysis is to extract the longwave component of the Bouguer anomaly derived from the deep subsurface composition as shown in Fig. 3-5.18. The trend surface is obtained by approximating the longwave component of the Bouguer anomaly by an n-order curved surface. Each coefficient is solved by applying least squares approximation to the Bouguer anomaly in the following equation:

- First order trend surface : $\Delta G_1(x, y) = a_0 + a_1 x + a_2 y$
- Second order trend surface : $\Delta G_2(x, y) = a_0 + a_1 x + a_2 y + a_3 x^2 + a_4 xy + a_5 y^2$
- N order trend surface :

$$\Delta G_n(x, y) = a_0 + a_1 x + a_2 y + a_3 x^2 + a_4 xy + a_5 y^2 + \cdots + a_{m-1} xy^{n-1} + a_m y^n$$

where m=n(n+3)/2

The n-order trend surface residual is obtained by subtracting the n-th trend surface from the Bouguer anomaly value ($\Delta g(x, y) - \Delta G(x, y)$)

5) Upward-continuation filter

The Bouguer anomaly at a given elevation is calculated by using the upward-continuation filter analysis. This process means that the Fourier coefficient of the wave number m of x direction and n of y direction is weighted by using the following equation.

$$w_{mn} = \exp\left(-\sqrt{(m^2 + n^2)}H\right)$$

The long wave component of the Bouguer anomaly can be extracted by using upward-continuation filter analysis. Upward-continuation filter analysis at two different heights can play the role of a band pass filter.

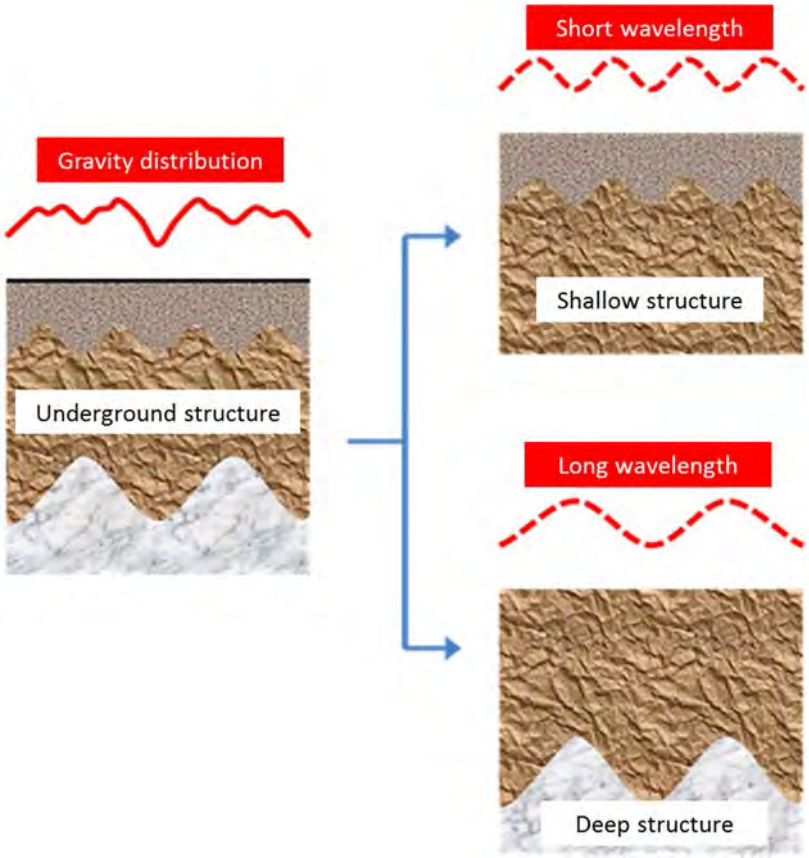

Source: JICA study team

Fig. 3-5.18 Conceptual diagram of trend surface analysis filter

6) Horizontal first derivation and vertical second derivation filter analysis

Fig. 3-5.19 shows a conceptual diagram of the horizontal first derivative and vertical second derivative. Horizontal derivative filtering is one of the high-pass filtering processes which emphasize the boundaries of the structures, using the horizontal first derivative values of the Bouguer anomaly. Based on the results of the horizontal first derivation, faults and/or intrusive rock can be detected. However, since density boundaries situated at shallow depths create a remarkably high anomaly in the horizontal derivative distribution, and deep-seated density boundaries only create a slightly high anomaly, the deep-seated density anomalies are easily overlooked. For this reason, the locations of points showing the maximum values of horizontal first derivative distribution were determined using a mathematical method, and the locations were used as additional information for detecting subsurface structures such as faults and/or intrusive rock (Fig. 3-5.19).

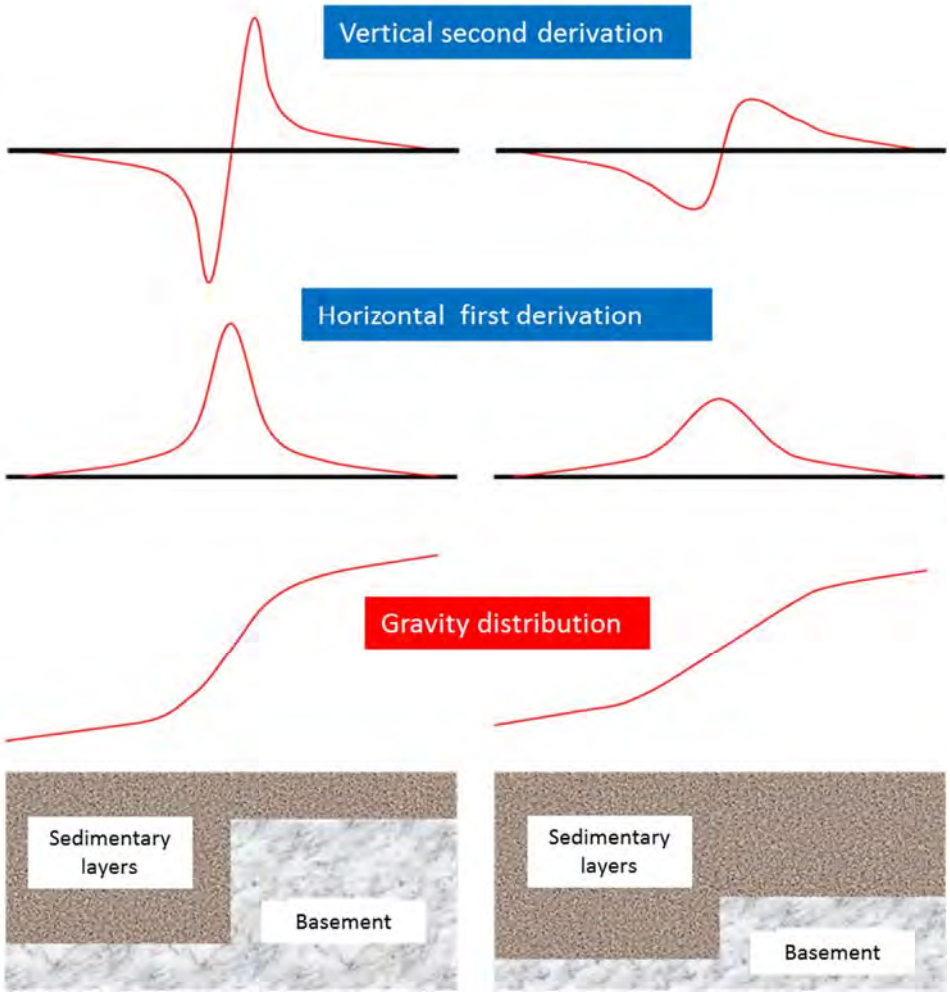

Source: JICA study team

Fig. 3-5.19 Conceptual diagram of vertical second derivation and horizontal first derivation

7) Three-dimensional gravity inversion of basement relief

The illustration below demonstrates the gravity value, which is caused by the rectangular-shaped body infinitely extending downward vertically, at a specific point (A, B, C)(Fig.3-5.20) can be calculated using the following equation (1).

$$G = \gamma\rho\{F(X1,Y1,Z) - F(X2,Y1,Z) - F(X1,Y2,Z) + F(X2,Y2,Z)\} \quad \cdots\cdots (1)$$

Where,

$$X1 = A - x1, \quad X2 = A - x2$$
$$Y1 = B - y1, \quad Y2 = B - y2$$
$$Z = |z - C|$$

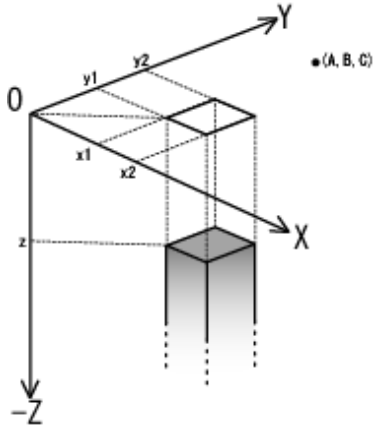

Fig. 3-5.20 Conceptual model of Three-dimensional gravity inversion of basement relief

$$F(x,y,z) = -\iiint \frac{z\,dx\,dy\,dz}{\left(x^2+y^2+z^2\right)^{3/2}}$$
$$= x\ln\left(\frac{y+\sqrt{x^2+y^2+z^2}}{\sqrt{x^2+z^2}}\right) + y\ln\left(\frac{x+\sqrt{x^2+y^2+z^2}}{\sqrt{y^2+z^2}}\right) - z\tan^{-1}\left(\frac{xy}{z\sqrt{x^2+y^2+z^2}}\right)$$

If the gravity stations and rectangular bodies representing the basement are aligned along the x and y coordinates in a grid system, a relative gravity anomaly, $\triangle G_{ij}(z)$ caused by the rectangular density body representing the basement relief can be calculated by equation (2).

$$\Delta G_{ij}(z) = \sum_k \sum_l \left\{ G_{ij}^{\ kl}(z, D_{kl}) - G_{ij}^{\ kl}(z, D_0) \right\} \quad \cdots\cdot(2)$$

Where,

D_{kl} : the depth of top of a rectangular body

D_0 : the average depth of basement relief

G_{ij}^{kl} : gravity value caused by rectangular density bodies at a station (x_i, y_i, z)

The initial approximation of the basement relief, D_{kl} is set using equation (3) for the gravity inversion.

$$D_{kl}^{(1)} = D_0 + \lambda \delta g_{ij} * / 2\pi\gamma\rho \quad \cdots\cdot(3)$$

Where,

δg* = observed gravity value – average value of all the observed gravity values

The gravity anomaly values at each station are determined by the initial density model and are calculated by using the following equation.

$$g_{ij}^{(1)} = \Delta G_{ij}(z_{ij}) = \sum_k \sum_l \left\{ G_{ij}^{\ kl}(z_{ij}, D_{kl}^{(1)}) - G_{ij}^{\ kl}(z_{ij}, D_0) \right\} \quad \cdots\cdot(4)$$

If an error sum of squares for $\delta g_{ij}^{(1)}$and δg* is sufficiently small, the D_{kl} will be a final density in the gravity inversion process. If the sum of squares is not sufficiently small, equation (3) is used to obtain the second approximation for the final density model.

$$D_{ij}^{(2)} = D_{ij}^{(1)} + \lambda\left(\delta g_{ij} * - \delta g_{ij}^{(1)}\right) / 2\pi\gamma\rho \quad \cdots\cdot(5)$$

Where

$\delta g_{ij}^{(1)} = g_{ij}^{(1)}$ – (an average value of $g_{ij}^{(1)}$)

After combining the equation (5) with equation (2), the following equation is derived.

$$g_{ij}^{(2)} = \Delta G_{ij}(z_{ij}) = \sum_k \sum_l \left\{ G_{ij}^{kl}(z_{ij}, D_{kl}^{(2)}) - G_{ij}^{kl}(z_{ij}, D_0) \right\}$$

An iterative least-square method is employed to determine the final basement relief model (depth of the top of each rectangular body, D_{kl}) until the error sum of squares for $\delta g_{ij}^{(1)}$ and δg^* become sufficiently small

(3) **Analysis results**

1) Bouguer anomalies

A Bouguer gravity anomaly map is shown in Fig. 3-5.21. As previously described, a rock density of 2.40g/cm^3 was used for calculating Bouguer anomaly values. The Bouguer anomaly values at each station are attached as an Appendix 2-6.

High-gravity anomaly zones are identified in and around the northwestern and the northeastern parts of the survey area. On the other hand, a low-gravity anomaly zone is distributed in and around the southwestern and the southern parts of the survey area. This low gravity anomaly zone extends from the southern part to the northwestern part of the survey area.

2) Trend surface analysis

Trend surface analysis was applied to obtain the regional trend of the gravity distribution. After utilizing five different orders of polynomial equations to estimated the regional trend of the gravity distribution, the regional trend derived from the third order equation was considered to be the most effective for separating the regional trend and the residual anomaly.

A trend surface map and a residual gravity map based on the results derived from the trend surface analysis are shown in Fig. 3-5.22 and Fig. 3-5.23 respectively. According to the trend surface map shown in Fig. 3-5.22, the high-gravity anomaly is identified in and around the northwestern and eastern parts of the survey areas, and the low-gravity anomaly is identified in and around the southwestern part of the survey areas. The trend surface of the Bouguer anomaly reflects the structure of the gravity basement.

The residual gravity values were calculated by deducing values of trend surface from Bouguer anomaly values. The residual gravity distribution is considered to reflect density distribution above the basement structure (Fig. 3-5.23). Based on the distribution of this residual gravity map, a gravity anomaly zone is distributed in the region from the northwestern part to the southeastern part of the survey area, and a high-gravity anomaly zone is recognized in the northern, southeastern and western parts of the survey area. On the other hand, a low gravity anomaly zone is identified from the central to southeast areas, and is also identified in the western, northwestern and northeastern parts of the survey area. The zone showing a steep gradient in residual gravity is located in between these low and high anomalies and the zone suggests a linearly distributed subsurface density discontinuity.

This kind of gravity discontinuity, linearly distributed, often reflects a fault or a fracture zone. This gravity discontinuity is often called a “gravity lineament”. To detect gravity lineaments, horizontal first derivative values were calculated using the residual gravity values. A map showing horizontal first derivative values of residual gravity is depicted in Fig. 3-5.24. High anomaly zones of the horizontal first derivative values indicate structures with large changes in density. Therefore, if a high anomaly zone of the horizontal first derivative values extends in a certain direction, a fault can be deduced around the high anomaly zone. On the basis of the distribution of the horizontal first derivative map, the following eight gravity lineaments were detected. In Fig.3-5.24, red broken lines show gravity lineaments extracted by the continuity of the high anomaly of the horizontal first derivative values. The northwestern part of the gravity lineament G1 cannot be extracted by the result of the first horizontal derivative analysis. The northwestern part of the lineament was extracted by gravity inversion of basement relief mentioned later.

- A clear gravity lineament which extends roughly in a NW-SSE direction and is located in the southern portion of the survey area (G1).
- A clear gravity lineament which extends roughly in a NW-SE direction and is located in the southeastern portion of the survey area (G2).
- A clear gravity lineament which extends roughly in a WNW-ESE direction and is located in the western portion of the survey area (G3).
- A clear gravity lineament which extends roughly in a NW-SE direction and is located in the central portion of the survey area (G4).
- A clear gravity lineament which extends roughly in a NE-SW direction and is located in the northeastern portion of the survey area (G5).
- A clear gravity lineament which extends roughly in a NE-SW direction and located in the northern portion of the survey area (G6).
- A clear gravity lineament which extends roughly in a NW-SE direction and is located in the northern portion of the survey area (G7).
- A clear gravity lineament which extends roughly in a NNE-SSW direction and is located in the northwestern portion of the survey area (G8).

3) Upward continuation analysis

The upward continuation method is a filtering technique which is different from the above-mentioned trend surface analysis. However, the purpose of the upward continuation analysis is similar to that of trend surface analysis, that is to separate a residual gravity anomaly from the original Bouguer anomaly distribution. In this study, the upward continuation method was applied to the Bouguer anomaly data to extract middle-scale and large-scale structures. The upward continuation method calculates a potential field at an elevation which is higher than the actual elevation where the gravity field was measured. Upward continuation is a kind of smoothing process to eliminate small-scale, near-surface density effects. Therefore, this analysis can remove small-scale noise structures at shallow depths from the Bouguer anomaly and thus the middle to large-scale structures are easily detected in the survey area. In this data analysis, the upward continuation was calculated at elevations of 100m and 3,000m above

the gravity stations. The values between 100m and 3000m were then determined by subtracting the values at 100m from the values at 3000m. This analysis has the effect of a band-pass filter removing both effects caused by the small-scale noise structures at shallow depths and the large-scale regional structures in and around the survey area. An upward continuation map (100m to 3,000m) is shown in Fig. 3-5.25.

The low gravity anomaly is distributed from the central to the southeastern part of the survey area as shown in the residual map of 3rd trend surface analysis (Fig.3-5.23). A high gravity anomaly in Fig. 3-5.25 is more clearly detected in the northwestern part of the survey area than the high gravity anomaly in Fig. 3-5.23. However, the distribution of the upward continuation values shown in Fig. 3-5.25 is similar to that in the above-mentioned residual gravity map.(Fig. 3-5.23). In the same way as for the above-mentioned trend surface analysis, the horizontal first derivative values were calculated using the upward continuation values for the purpose of extracting fault structures. The horizontal first derivation map calculated from the upward continuation is shown in Fig. 3-5.26. Based on the distribution of the horizontal first derivative map, the following gravity lineaments were detected. The red broken lines in Fig. 3-5.26 are same as the lines in Fig. 3-5.24.

- A clear gravity lineament which extends roughly in a NW-SSE direction and is located in the southern portion of the survey area (G1).
- A clear gravity lineament which extends roughly in a NW-SE direction and is located in the southeastern portion of the survey area (G2).
- A clear gravity lineament which extends roughly in a WNW-ESE direction and is located in the western portion of the survey area (G3).
- A gravity lineament which extends roughly in a NW-SE direction and is located in the central portion of the survey area (G4).
- A clear gravity lineament which extends roughly in a NE-SW direction and is located in the northeastern portion of the survey area (G5).
- A gravity lineament which extends roughly in a NE-SW direction and located in the northern portion of the survey area (G6).
- A clear gravity lineament which extends roughly in a NW-SE direction and is located in the northern portion of the survey area (G7).
- A clear gravity lineament which extends roughly in a NNE-SSW direction and is located in the northwestern portion of the survey area (G8).

The above-mentioned gravity lineaments detected in the distribution of the horizontal first derivative using upward continuation (100m to 3,000m) are almost same as those detected in the distribution of the horizontal first derivative using the residual gravity data derived from trend surface analysis. In first horizontal derivative analysis of upward-continuation, gravity lineaments G4 and G6 were not extracted clearly like in Fig. 3-5.24, but the distribution of the maximum value of first horizontal derivative analysis is similar to Fig. 3-5.24. This fact means that the same gravity lineaments were detected by different data analyses, and therefore these gravity lineaments are reliable and may indicate faults.

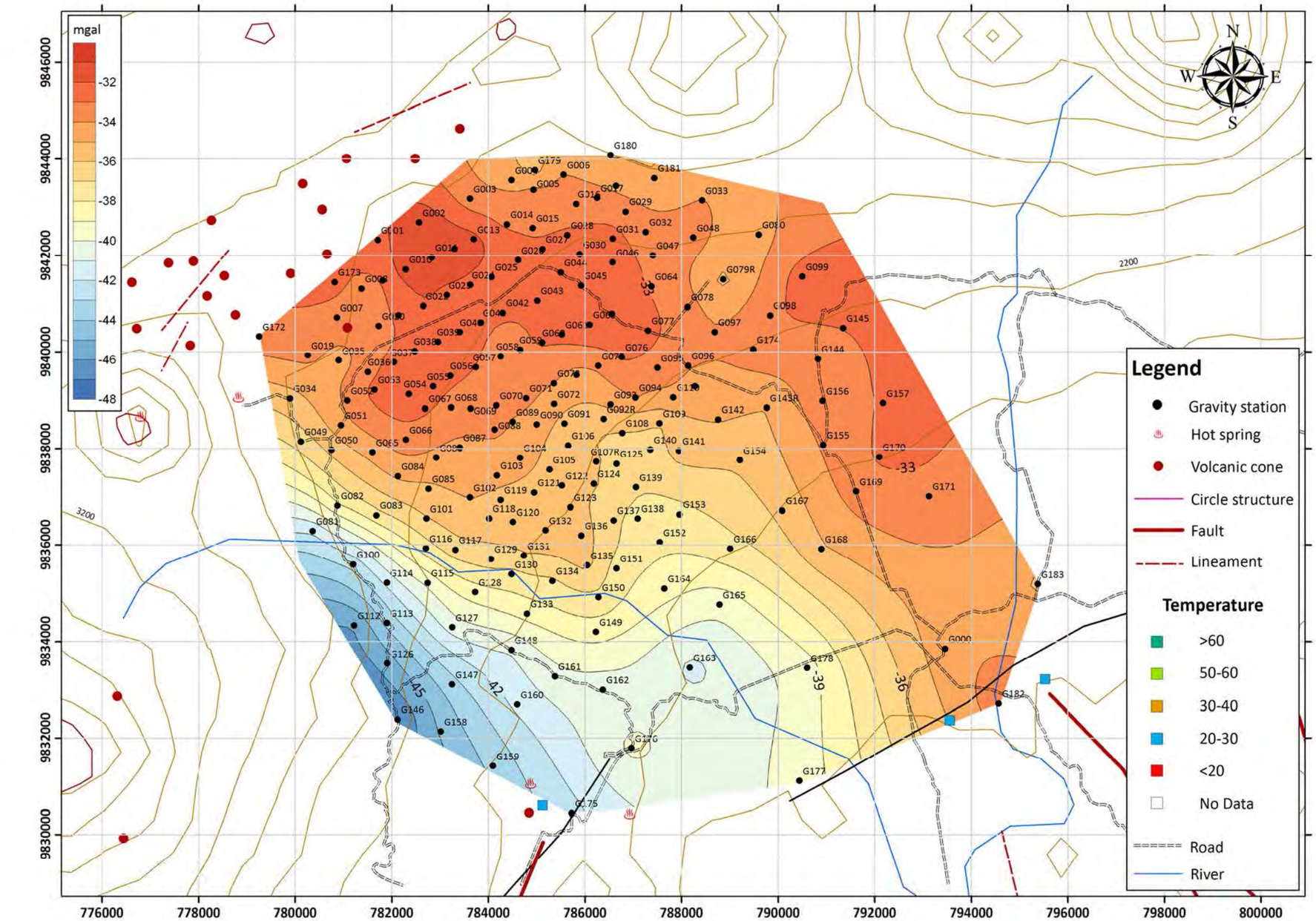

Source: JICA study team

Fig. 3-5.21 Bouguer anomalies map（Density；2.40g/cm3）

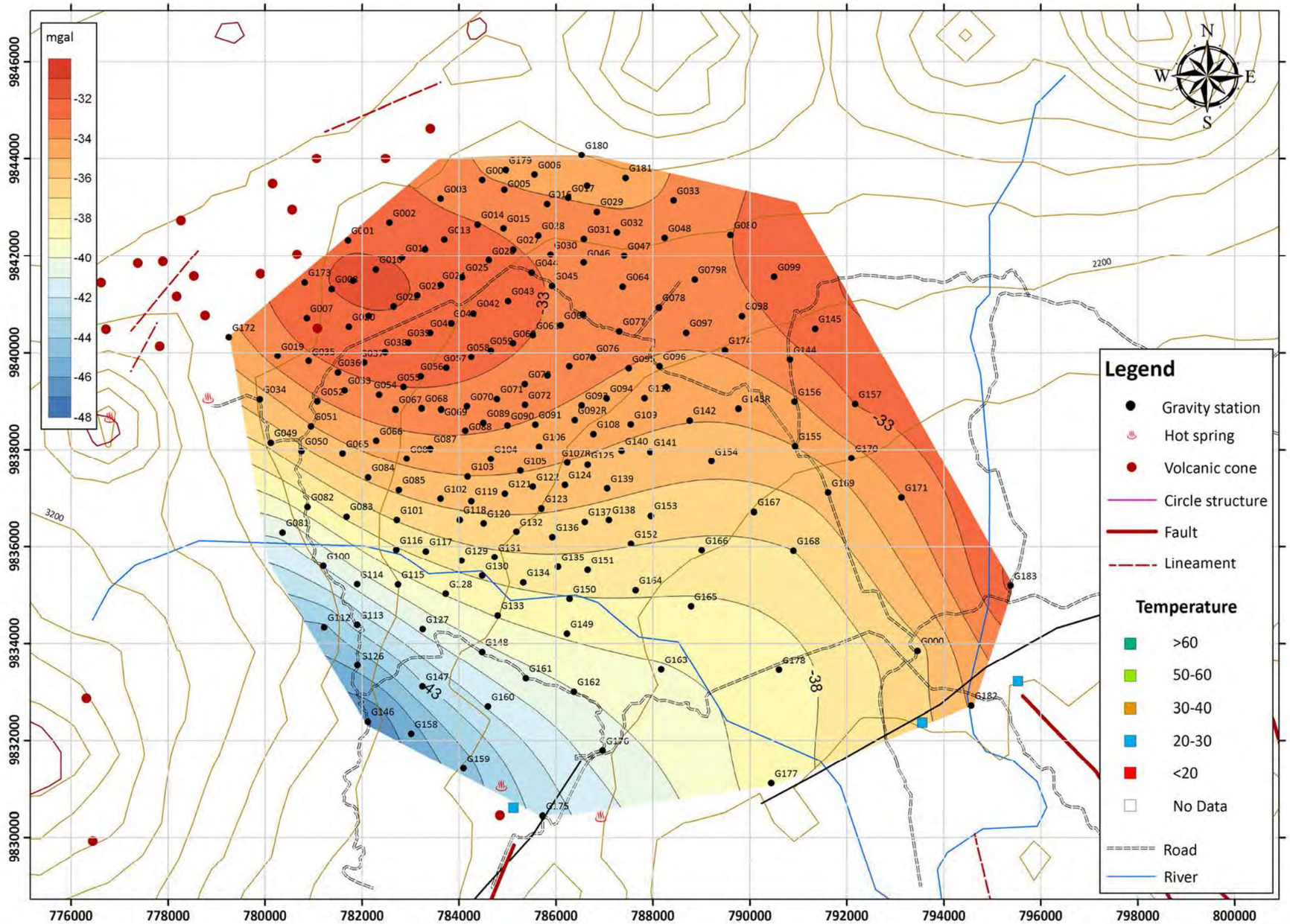

Source: JICA study team

Fig. 3-5.22 3rd Trend surface map

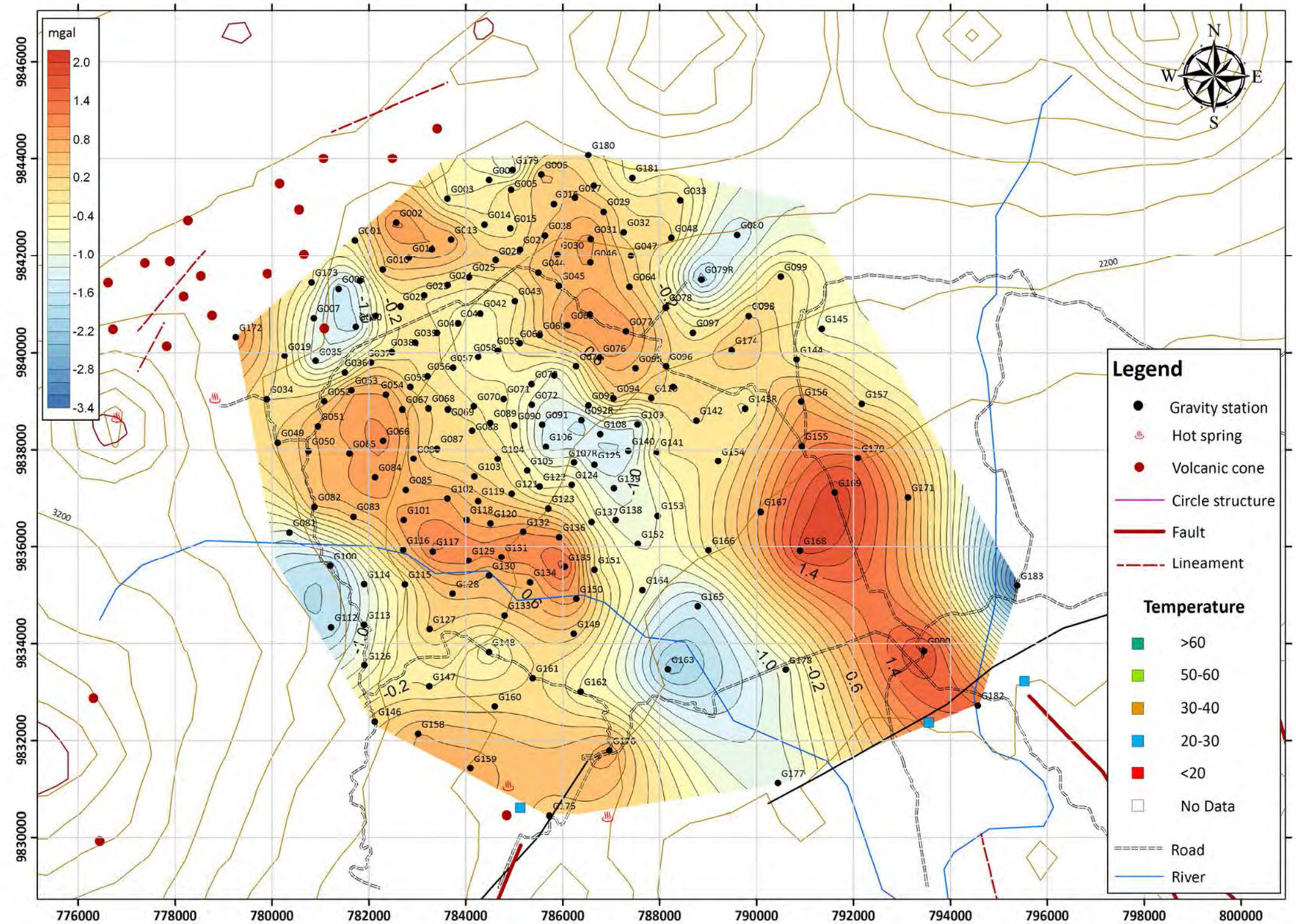

Source: JICA study team

Fig. 3-5.23 Residual of 3rd trend surface map

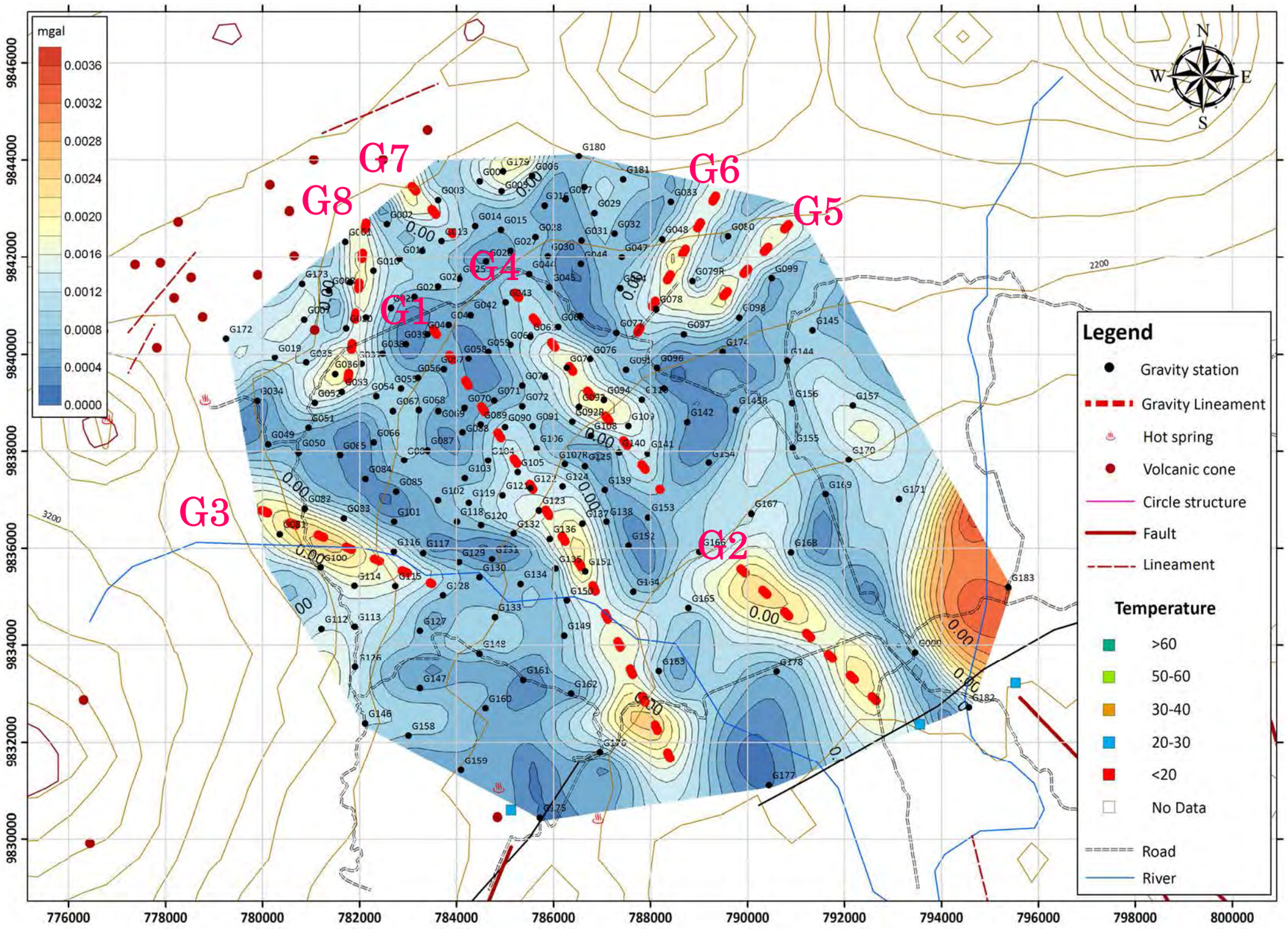

Source: JICA study team

Fig. 3-5.24 Horizontal first derivation of residual of 3rd trend surface map（S=500m）

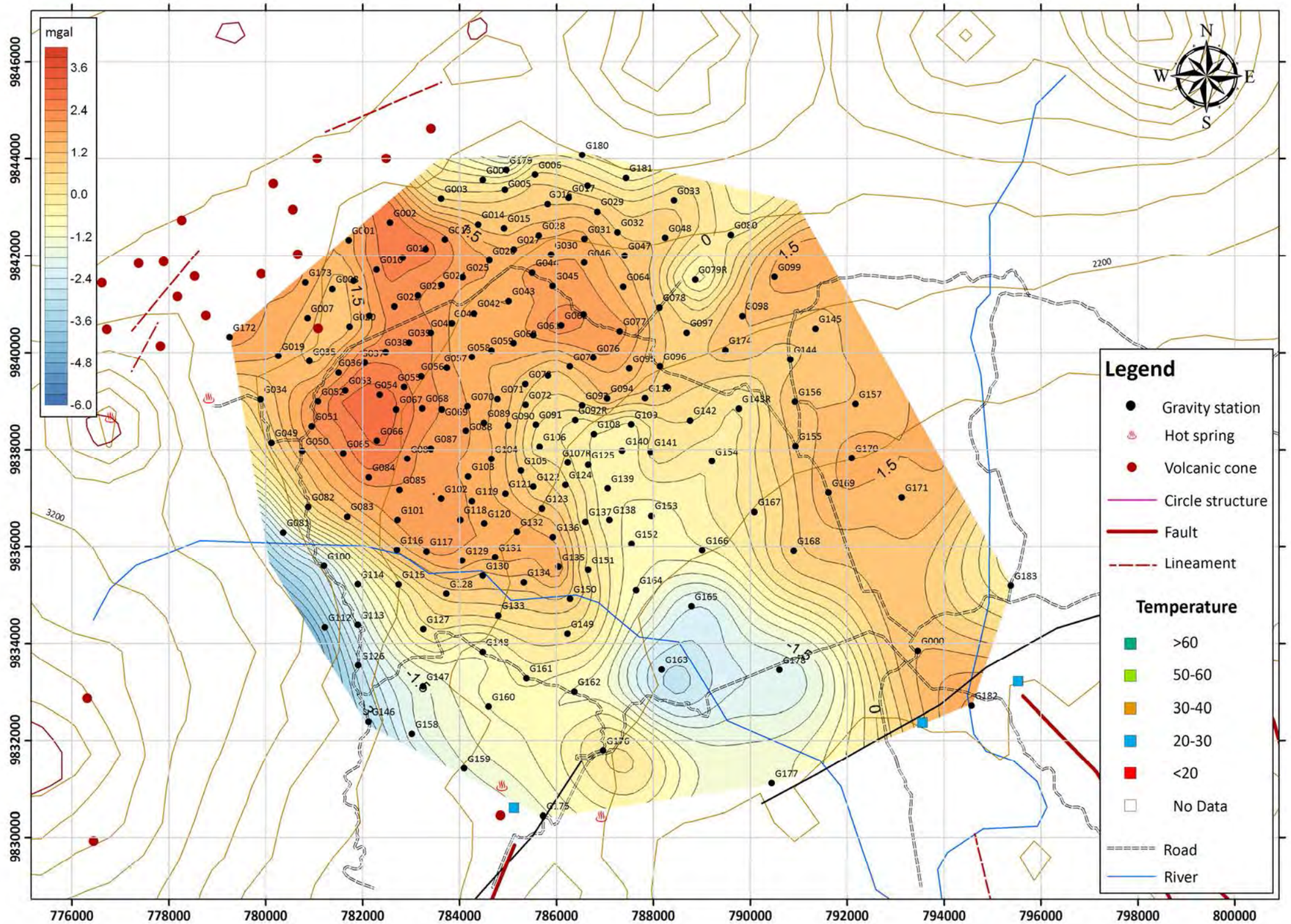

Source: JICA study team

Fig. 3-5.25 Upward continuation map（100~3000m）

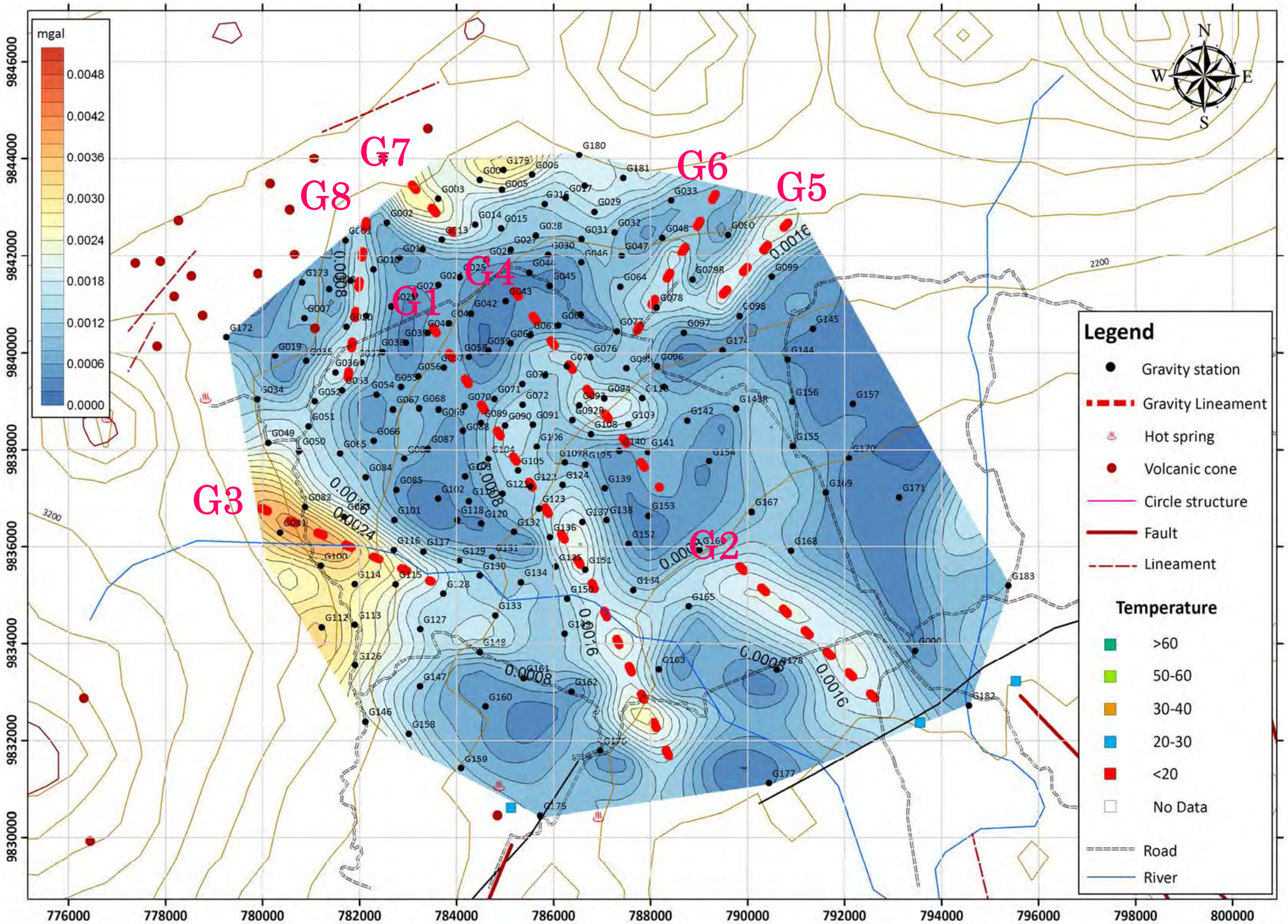

Source: JICA study team

Fig. 3-5.26 Horizontal first derivation map（S=500m）of upward continuation（100~3000m）

4) Gravity inversion of basement relief

A gravity inversion of basement relief was conducted to estimate the depth distribution of the top of deep-seated basement rock in the survey area. During the inversion process, the value of the density difference between the basement rock and volcanic rocks overlaying the basement is required to estimate a proper basement relief. However, no information is available for densities of rock in and around the survey area. Therefore, geophysical papers describing rock density, derived from other gravity surveys in African countries, were examined. In the paper "Integrated Geophysical Study of Lake Bogoria Basin, Kenya: Implications for Geothermal Energy Prospecting, Josphat Mulwa et al., Proceedings World Geothermal Congress 2010", rock densities were determined by data analysis. Based upon those rock densities, the density difference can be assumed to be 0.3g/cm^3 in the Kinigi field.

Fig. 3-5.27 shows the result of the gravity inversion of basement relief. The red broken lines in Fig. 3-5.27 show the same gravity lineament as Figs. 3-5.24 and 3-5.26. The parts where there is steep change in the top of the basement elevation, which often indicates underground structures such as faults, accord with the gravity lineaments (G1~G8). The elevation of the top of the basement near the low gravity anomaly zone from the central to the southeastern parts of the survey area is deep and the steep parts roughly correspond to the gravity lineaments G1, G2 and G4. Thus the gravity lineament G1, G2 and G4 may indicate faults located around the edge portion of the basement depression. The western part of the basement depression extends way down the northwest compared with the high anomaly zone of the first horizontal derivative values in Figs. 3-5.24 and 3-5.26, so gravity lineament G1 was detected by the gravity inversion of basement relief.

Since the precise density difference between the basement and volcanic rocks overlying the basement is unknown, and no control point for basement depth is available, the distribution of the basement depth was not accurately determined in the gravity inversion process. Based on the basement depth distribution derived from the gravity inversion with the above-mentioned assumption of the density difference, an average basement depth in the graben is estimated to be approximately 2,000 m from the ground surface.

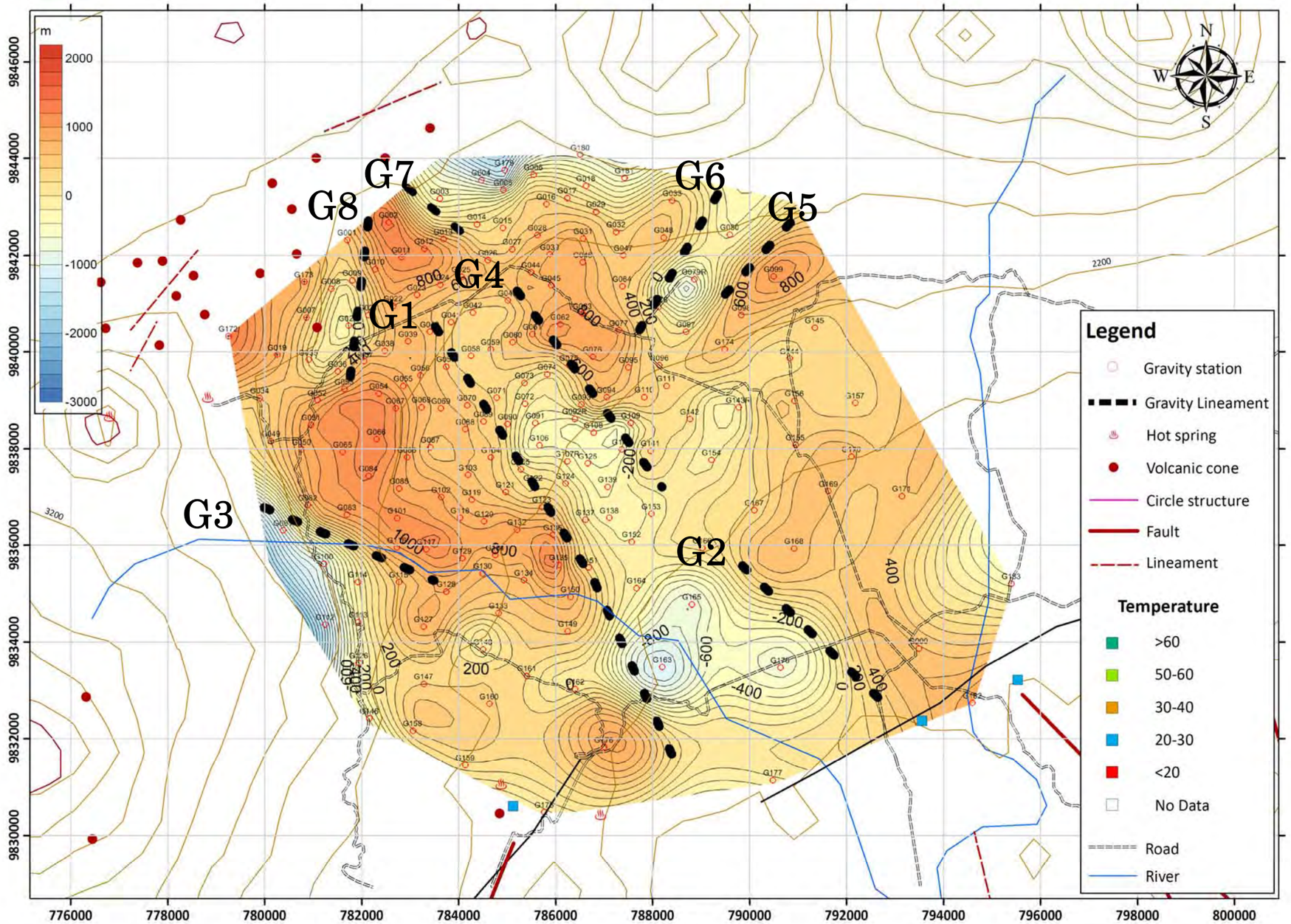

Source: JICA study team

Fig. 3-5.27 Basement relief derived from gravity inversion

5) Gravity analysis of the selected area

MT data was acquired in Kinigi field prior to this project and three-dimensional resistivity inversion was performed in the second phase of this project. On the basis of the results of three-dimensional resistivity inversion, a low resistivity zone of less than 10 ohm-m is recognized in the northern part of the Kinigi field at a depth of 2,000m and deeper. In order to better understand details of the underground structure, trend surface analysis and horizontal first derivative analysis were performed for the selected gravity data in and around the low resistivity zone detected from MT data analysis.

Fig. 3-5.28 shows the residual map of 2nd trend surface analysis. Gravity lineaments G1~G8 mentioned previously are described in Fig. 3-5.28. A high gravity anomaly is clearly distributed in the northwestern part of the survey area, while on the other hand a low gravity anomaly is distributed in southeastern part of the survey area and is aligned in a NW-SE direction. The gravity residual is distributed from northwest to southeast, and this trend is the same as in the residual map of 3rd trend surface analysis. (Fig. 3-5.23)

Horizontal first derivative values were calculated using the residual values for detecting underground structure such as faults. Fig. 3-5.29 shows the result of the horizontal first derivative. Based on the distribution of the horizontal first derivative map, the following three gravity lineaments were detected.

- A gravity lineament which extends roughly in a ENE-WSW direction and is located in the northern portion of the survey area (G9).
- A gravity lineament which extends roughly in a ENE-WSW direction and is located in the northern portion of the survey area (G10).
- A gravity lineament which extends roughly in a NW-SE direction and is located in the western portion of the survey area (G11).

The extracted gravity lineaments G9 and G10, and the northern part of the gravity lineament G1 mentioned before are located in and around the low resistivity zone which possibly refrect hydrothermally altered zone, and thus these gravity lineaments may control the flow of geothermal fluid at depth.

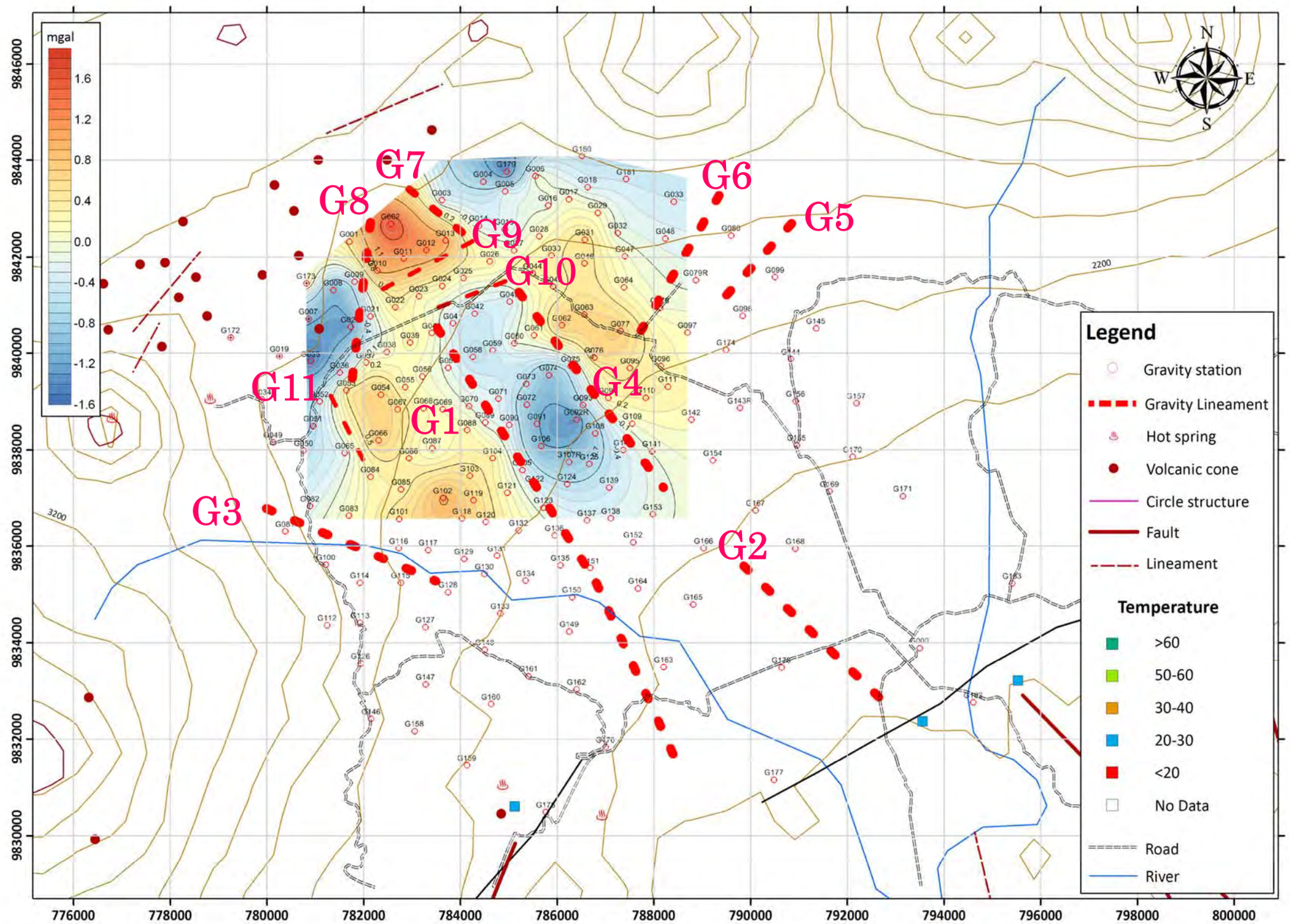

Source: JICA study team

Fig. 3-5.28 Residual of 2nd trend surface map

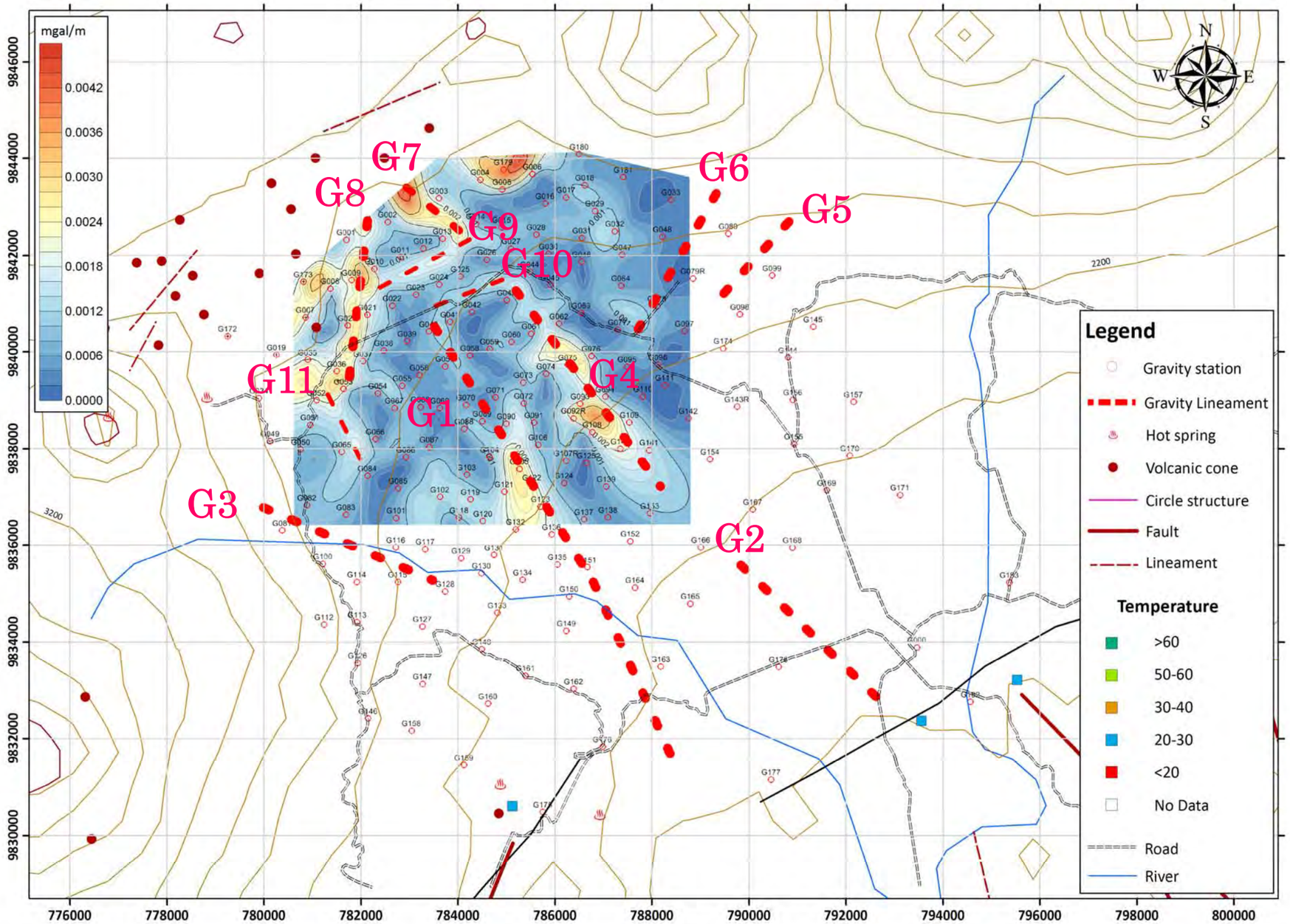

Source: JICA study team

Fig. 3-5.29 Horizontal first derivation of residual of 2nd trend surface map

(4) **Technical transfer of gravity survey techniques**

Technology transfer related to gravity survey techniques was carried out as follows.

- ✓ Performed place: Kinigi and EDCL/GU office
- ✓ Performed date: September 27-October 1 (4 days)
- ✓ Purpose: Understanding the acquisition of gravity survey data and the techniques for analyzing it.

During the technical transfer, existing gravity data acquired in the Bugarama field was utilized. The following technical transfers to the REG were performed by the JICA team members.

- ➢ Explanation regarding the content and schedule of this technical transfer
- ➢ On-the-job training regarding gravity data acquisition
- ➢ On-the-job training regarding gravity data processing including data correction
- ➢ On-the-job training regarding the filtering processes (trend surface analysis, band-width filtering process using the upward continuation method, horizontal derivative analysis, etc.)
- ➢ Explanation regarding how to use the SURFER software.
- ➢ On-the-job training regarding the three-dimensional gravity inversion technique using a 2 layer density model (creation of input files, parameter settings, creation of depth map of the estimated basement rock derived from the inversion, etc.)
- ➢ On-the-job training regarding extracting subsurface structures (faults, intrusive rock, etc.) in light of the results of gravity data analysis

- ✓ Participants: Jean d'Amour (Geophysicist), Gatean SAKINDI (Geophysicist), Jean Jacques HAVUGIMANA (Geophysicist)

Photo 3-5.2 Condition for technical transfer of gravity survey techniques

3.5.3. Technology transfer related to the geothermal conceptual model update

(1) Update for geothermal conceptual model of Kinigi

A comprehensive analysis map of Kinigi and geothermal conceptual model are shown in Fig. 3-5.30 and Fig. 3-5.31 respectively. This geothermal conceptual model was created as part of the update support through the capacity building.

1) Geological structure

Kinigi is geologically composed of Proterozoic basement rocks and Quaternary volcanic rocks. In general these rocks are not permeable, and therefore zones of permeable fractures extending at depth are where geothermal fluids may be stored. According to the reanalysis of MT data, a widely distributed low resistivity zone is clearly detected at a depth of 2,000 m and deeper in the northern portion of Kinigi. In addition, two remarkable resistivity discontinuities, R2 and R3 can be identified at a depth of 1,500 m and deeper in and around the areas of the eastern edge and the western edge of the remarkable low resistivity zone, respectively. Also, NNW-SSE trending gravity lineaments are distributed in the study area. Geological structures in the southern part of Kinigi (in the Butare Horst) are characterized by the presence of NNW-SSE trending faults. The geological structures R2 and R3 delineated by 3D MT inversion and the gravity lineaments G1 and G4 show the presence of NNW-SSE trending faults (F1, F2 and F3) developed in the Proterozoic basement seated below the volcanic rock. Cone volcanics are distributed in a NE-SW orientation between the Visoke volcano and Sabyinyo volcano. In addition, gravity lineaments G9 and G10 are distributed in the same orientation as the structure in the northern part of the study area. This suggests the possibility of the presence of a deep-seated fracture system.

2) Geothermal structure

It is obvious to think that a heat source exits beneath a volcano; however, depending on the age, depth and size of the presumed heat source it may or may not be the center of activity for a geothermal system. There are clues to discern whether or not the magmatic intrusion beneath a volcano is a relevant source of energy. In the Kinigi field, a large number of Quaternary volcanic activities occurred on the Proterozoic granite and the phyllite basement rocks. Young volcanoes include cone volcanoes, Sabinyo volcano, Gahinga volcano, Visoke volcano and Karisinbi volcano. Most of these volcanoes are composed of alkali basalt; in general the magma of these basaltic rocks tends to be located at great depths. In addition, a number of cone volcanoes, which are situated in the northern part extend in a NE-SW direction. It is presumed that a basaltic dyke has intruded at the shallow depth. On the other hand, an andesitic volcanic rock has erupted at Visoke and Sabyinyo volcanoes. Basaltic lavas erupted in the first stage of volcanic activity, and then andesitic lavas erupted in the second stage. K-Ar rock dating of the andesite is obtained as 0.5 to 1.0 Ma in this project. These analytical results suggest the possibility that a magma chamber existed in the late Quaternary and could be a heat source of a geothermal system which exists at relatively shallower depths in and around Mt. Sabyinyo. Although Visoke volcano likewise is andesitic, when considering the scale of the volcanic bodies, the most promising heat source for geothermal activity in Kinigi would be Sabyinyo volcano.

A widely distributed low resistivity zone is clearly detected at a depth of 2,000 m and deeper in the northern portion of Kinigi in the reanalysis of MT data. The low resistivity zone in the northern portion of Kinigi may be the result of argillized rock affected by geothermal activity and containing considerable amounts of smectite and/or interstratified clay minerals. In this case, fault F1 (resistivity discontinuity R2) and F3 (R3) probably reflect fracture zones at depth. A slightly lower resistivity zone is distributed on the northeast side of F3. On the other hand, a high resistivity zone is widely distributed on the southwest side of F1. These resistivity structures are similar to those to the south of Karisimbi volcano (in Karisimbi) which were shown through reanalysis of MT data. Therefore, they are considered likely to exhibit a similar geothermal structure, indicating that this high resistivity zone has a less permeable rock body where fractures are not well developed. Actually, the underground temperature of exploration well KW-01, which was drilled in the area south of Karisimbi volcano, was low and it did not provide information suggesting a high permeability zone.

3) Geothermal fluid flow

No geothermal manifestations such as fumaroles, hot springs, or altered ground have been recognized in the Kinigi field. Cold springs such as Rubindi, Mubona, Cyabararika, etc. are found at the topographic boundary of the volcanic region in the north and the Butare Horst in the south. The cold spring water contains CO_2 gas. These springs are classified into neutral high HCO_3 type water with temperature around 20°C and with a relatively high bicarbonate (HCO_3) concentration at a maximum of 2,260mg/L. It is estimated that these spring water is not contaminated by deep hot water, but rather that the CO_2 has been added to the shallow ground water. In addition, the strontium isotope of the spring water is similar to the strontium isotope of Virunga volcanic rocks (IESE, 2012), and it is therefore estimated that the spring water flows through the volcanic rocks. Since these spring water does not reflect information concerning the deep subsurface fluid, it is unclear about the properties of the geothermal fluid

NNW-SSE trending faults are developed in the Proterozoic basement seated below the volcanic rock in the Kinigi field. If there are permeable fracture zones around these faults, it is considered that geothermal fluid is stored in the fracture zone and an alteration zone identified by a low resistivity zone is generated by geothermal fluid. Precipitation at high elevation in this area penetrates deep into the ground through the faults of mainly NE-SW orientations in the study area, and is heated by magma. However this suggests that even if geothermal fluids are stored along the permeable fracture zone around faults in the northern portion of Kinigi, the temperature of the geothermal fluids may not be high enough for conventional type geothermal power generation.

(2) **Technology transfer related to the geothermal conceptual model update**

Technology transfer related to the geothermal conceptual model update was conducted as follows.

- ✓ Performed place: Kigari EDCL/GDU office
- ✓ Performed date: February 5 , 2016
- ✓ Purpose: Understanding of the method of geothermal conceptual model update
- ✓ Participants: Ms.Uwera RUTAGARAMA (Reservoir Engineer), Mr. Jean Pascal NIYIGENA

(Geochemist), Mr. Jean Jacques HAVUGIMANA (Geophysicist), Mr. Theoneste NZAYISENGA (Drilling Engineer)

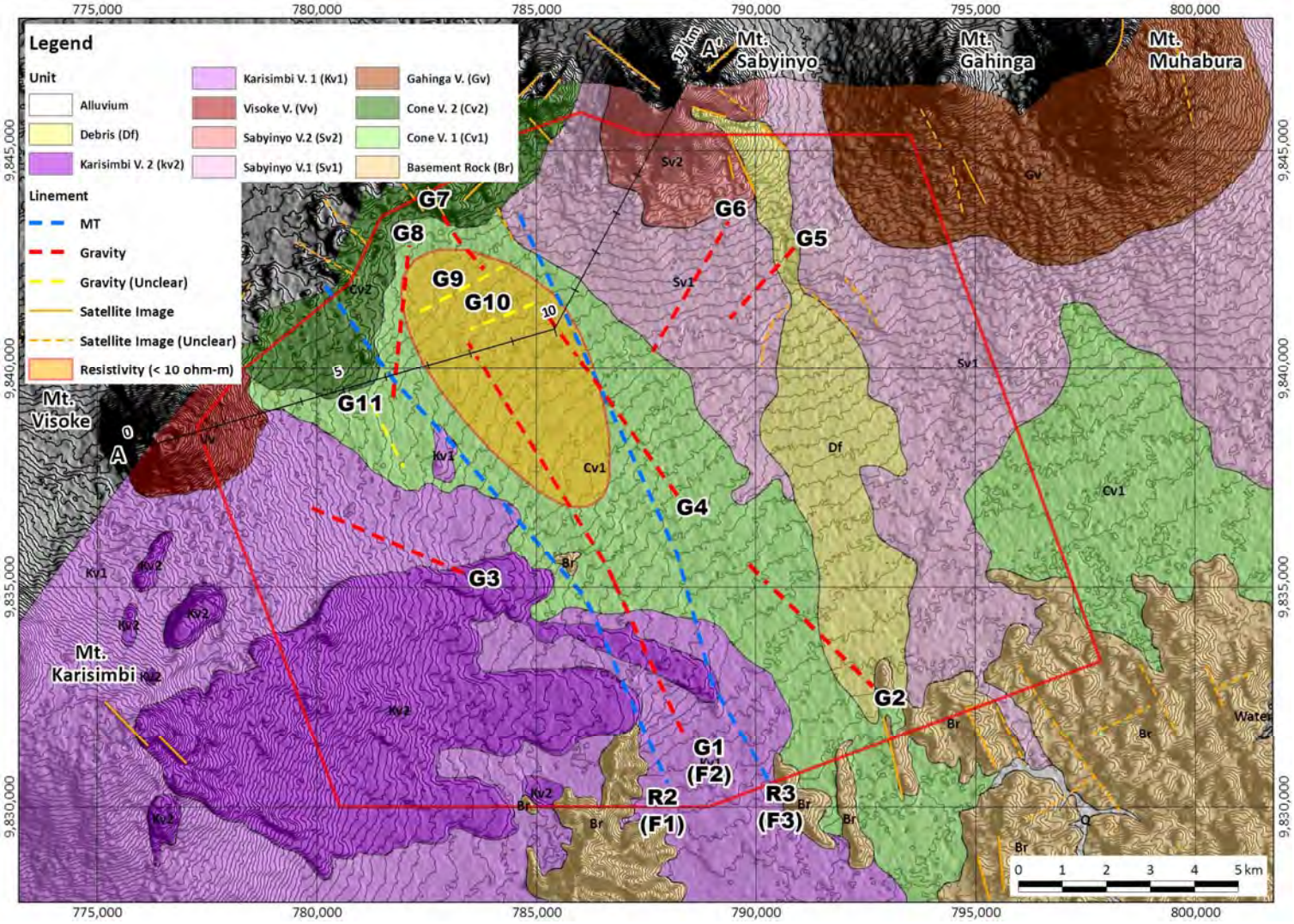

Source: JICA study team

Fig. 3-5.30 Geological map of Kinigi field

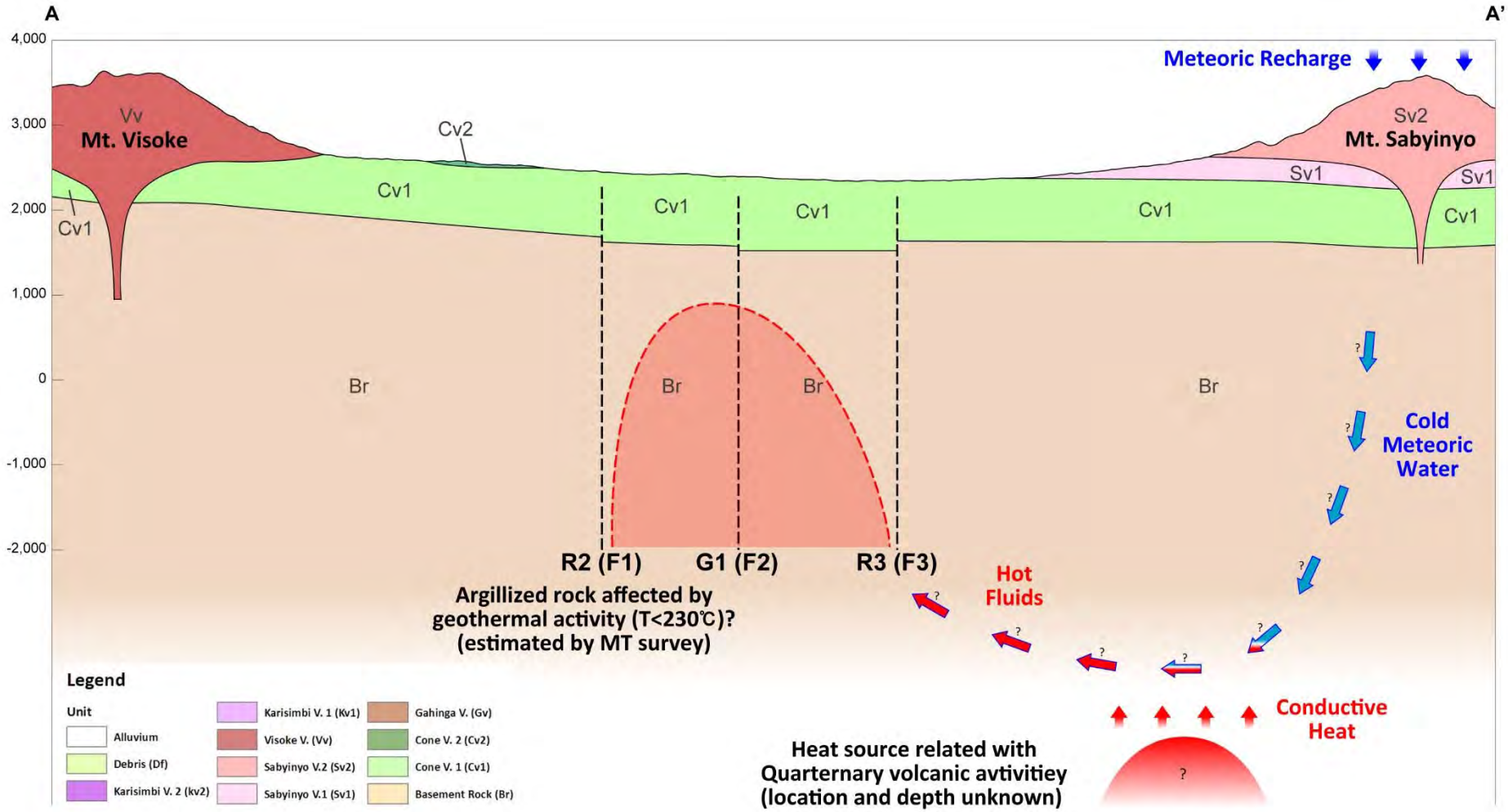

Source: JICA study team

Fig. 3-5.31 Geological cross section of Kinigi field

3.6. Recommendation on Formulation of Geothermal Development Plan

Even in the Kinigi and Bugarama fields, the presence of a geothermal reservoir adequate for power generation has not yet been confirmed, so the resource development risk is thought to be relatively high. However, a tentative geothermal development plan was formulated as a reference for Kinigi and Bugarama fields, which were ranked as having the highest priority for exploration activity in Rwanda. The earliest commencement of power generation will be 2023 in Bugarama field.

In Kinigi field, it is assumed that about 10 years will be necessary to commencement from the selection of the consultant for "Phase 2". However, these formulated development plans were based on results of resource potential evaluation as of 2nd year work. These provisional estimate does not always correctly indicate the sustainable optimum power output at that point.

Particularly, the geothermal conceptual model of Kinigi field constructed in the 3rd year of this project may not provide clear evidence for the interpretation of the resistivity construction and the geothermal system (fluid temperature in basement rock etc), so the low possibility of the presence of geothermal fluid cannot be denied. Furthermore, even when geothermal fluid is present along the permeable zone around faults, it is assumed that the presence of high temperature geothermal fluid around the permeable zone is low. Therefore, in case of drilling exploration wells, the possibility that the wells will not self-discharge may not be denied. Based on the above, large scale geothermal power generation may not be possible in this area. In this regard, the surveys in this project did not provide confirmatory information regarding the existence of a geothermal reservoir. Considering the results of these surveys, the geothermal development risk in Kinigi field is determined to be high. Furthermore, if the next step in exploration is decided to be undertaken, even though geothermal development risk need to be fully considered as described above, exploration well shall be drilled to confirm the underground structure and the existence of geothermal reservoir.

Considering this current situation of geothermal development in Rwanda, the JICA study team describe recommendation and issues of concerns for future geothermal development activity in Rwanda as follows.

- Some technical tasks in the assessment of the geothermal resource remain because an exploitable geothermal reservoir has not been confirmed by drilling in all geothermal fields in Rwanda. Data presently available for all prospects are not sufficient to evaluate the geothermal resource and the presence of a geothermal reservoir adequate for power generation has not yet been confirmed. Therefore, geothermal exploration study is required for the judgment of resource feasibility of geothermal power development in Rwanda.
- Geothermal resource evaluation based on exploratory well drilling and production testing in the next stage (Phase 3) is required to identify the optimum sustainable power output. It should be noted that the details of geothermal power plant projects should be formulated in a feasibility study, which will be carried out later on the basis of the geothermal resource study (Phase 3).
- In this study, exploration studies necessary for above-mentioned judgment in Phase-2 and Phase-

3 are formulated as an action plan. It is desirable that resource assessment will be done at each Phase and judgments at each Phase would be required to progress next stage or not in all fields.

- Government-led surveys corresponding to Phase 2 and Phase 3 are desired to confirm the presence of geothermal reservoirs and to promote geothermal development in this country, because the resource development risk is thought to be relatively high. It is recommended that support by the donors in this situation is best directed to enabling these early-stage surveys by the government or governmental agencies (REG).
- Support for capacity building among policy makers and/or survey staff involved in early stage development is important. In strengthening the capacity of REG, the following issues shall be considered.
  - ✓ Capacity building in geothermal exploration technology (geology, geophysics, geochemistry, reservoir engineering and environmental study) through geothermal exploration activity and through participation in training courses such as those held in Japan, New Zealand, Iceland, Kenya. Practical training through collaborative study is necessary. In this project, capacity buildings in geology, geochemistry and geophysics etc was carried out.
  - ✓ Management of geothermal resource and development database
  - ✓ Capacity building and supervision of project planning and management including procurement procedure, financial aspects etc.
  - ✓ Enrichment of basic survey equipment and software for geothermal investigation and analysis